NAVAL POSTGRADUATE SCHOOL

MONTEREY, CALIFORNIA

THESIS

THE SHIBOARD EMPLOYMENT OF A FREE ELECTRON LASER WEAPON SYSTEM

by

Gregory G. Allgaier

December 2003

Thesis Advisor: William Colson
Second Reader: Robert Armstead

Approved for Public Release; Distribution is Unlimited

THIS PAGE INTENTIONALLY LEFT BLANK

REPORT DOCUMENTATION PAGE			Form Approved OMB No. 0704-0188
Public reporting burden for this collection of information is estimated to average 1 hour per response, including the time for reviewing instruction, searching existing data sources, gathering and maintaining the data needed, and completing and reviewing the collection of information. Send comments regarding this burden estimate or any other aspect of this collection of information, including suggestions for reducing this burden, to Washington headquarters Services, Directorate for Information Operations and Reports, 1215 Jefferson Davis Highway, Suite 1204, Arlington, VA 22202-4302, and to the Office of Management and Budget, Paperwork Reduction Project (0704-0188) Washington DC 20503.			
1. AGENCY USE ONLY ***(Leave blank)***	**2. REPORT DATE** December 2003	**3. REPORT TYPE AND DATES COVERED** Master's Thesis	
4. TITLE AND SUBTITLE: The Shipboard Employment Of A Free Electron Laser Weapon System			**5. FUNDING NUMBERS**
6. AUTHOR(S) Allgaier, Gregory G.			
7. PERFORMING ORGANIZATION NAME(S) AND ADDRESS(ES) Naval Postgraduate School Monterey, CA 93943-5000			**8. PERFORMING ORGANIZATION REPORT NUMBER**
9. SPONSORING /MONITORING AGENCY NAME(S) AND ADDRESS(ES) N/A			**10. SPONSORING/MONITORING AGENCY REPORT NUMBER**
11. SUPPLEMENTARY NOTES The views expressed in this thesis are those of the author and do not reflect the official policy or position of the Department of Defense or the U.S. Government.			
12a. DISTRIBUTION / AVAILABILITY STATEMENT Approved for public release; distribution is unlimited.			**12b. DISTRIBUTION CODE**

13. ABSTRACT ***(maximum 200 words)***

A megawatt (MW) class Free Electron Laser (FEL) shows promise as a new weapon for anti-ship cruise missile defense. An FEL weapon system delivers energy at the speed of light at controllable energy levels, giving the war fighter new engagement options. Considerations for this weapon system include employment, design, and stability. In order to reach a MW class laser, system parameters must be optimized and the high power optical beam must be appropriately managed.

In a high power FEL, the optical beam could heat and ultimately damage the optical cavity mirrors. One proposed solution is a short Rayleigh length design, which lowers the intensity on the mirrors, but increases sensitivity to vibrations. This thesis shows a that short Rayleigh length FEL will remain stable using current technology and can be designed to achieve a MW of power. Scenarios are then presented to explore some of the engagement options associated with this weapon system.

14. SUBJECT TERMS Free Electron Laser, Short Rayleigh Length, Directed Energy, Mirror Stablity			**15. NUMBER OF PAGES** 88
			16. PRICE CODE
17. SECURITY CLASSIFICATION OF REPORT Unclassified	**18. SECURITY CLASSIFICATION OF THIS PAGE** Unclassified	**19. SECURITY CLASSIFICATION OF ABSTRACT** Unclassified	**20. LIMITATION OF ABSTRACT** UL

NSN 7540-01-280-5500 Standard Form 298 (Rev. 2-89)
Prescribed by ANSI Std. 239-18

THIS PAGE INTENTIONALLY LEFT BLANK

Approved for public release; distribution is unlimited.

THE SHIPBOARD EMPLOYMENT OF A FREE ELECTRON LASER WEAPON SYSTEM

Gregory G. Allgaier
Lieutenant, United States Navy
B.S., Armstrong Atlantic State University, 1996

Submitted in partial fulfillment of the
requirements for the degree of

MASTER OF SCIENCE IN APPLIED PHYSICS

from the

NAVAL POSTGRADUATE SCHOOL
December 2003

Author: Gregory G. Allgaier

Approved by: William B. Colson
Thesis Advisor

Robert L. Armstead
Second Reader/Co-Advisor

James H. Luscombe
Chairman, Department of Physics

THIS PAGE INTENTIONALLY LEFT BLANK

ABSTRACT

A megawatt (MW) class Free Electron Laser (FEL) shows promise as a new weapon for anti-ship cruise missile defense. An FEL weapon system delivers energy at the speed of light at controllable energy levels, giving the war fighter new engagement options. Considerations for this weapon system include employment, design, and stability. In order to reach a MW class laser, system parameters must be optimized and the high power optical beam must be appropriately managed.

In a high power FEL, the optical beam could heat and ultimately damage the optical cavity mirrors. One proposed solution is a short Rayleigh length design, which lowers the intensity on the mirrors, but increases sensitivity to vibrations. This thesis shows a that short Rayleigh length FEL will remain stable using current technology and can be designed to achieve a MW of power. Scenarios are then presented to explore some of the engagement options associated with this weapon system.

THIS PAGE INTENTIONALLY LEFT BLANK

TABLE OF CONTENTS

LIST OF FIGURES

THIS PAGE INTENTIONALLY LEFT BLANK

LIST OF SYMBOLS

a	dimensionless optical field strength
$\vec{A}$	vector potential
B	magnitude of the undulator magnetic field
$\vec{B}$	vector sum of the undulator and optical magnetic fields
$\vec{B}_S$	optical magnetic field
$\vec{B}_U$	undulator magnetic field
c	speed of light
e	charge of an electron
E	magnitude of the optical electric field
E_b	electron beam energy
E_e	electron energy
E_o	optical beam energy
$\vec{E}_S$	optical electric field
F	filling factor
G	optical gain
h	air contact altitude
H	height of sensor
j	dimensionless electron current
$\vec{J}_\perp$	transverse current density
k	optical wave number
k_0	undulator magnetic wave number
K	undulator parameter
l_b	electron bunch length
L	undulator length
m	electron mass
N	number of undulator periods
N_e	number of electrons
q	bunch charge
Q_n	resonator quality factor
$\vec{r}$	position vector
r_b	electron beam radius
R	radar horizon range
S	resonator length
t	time
v_z	electron longitudinal velocity
V	volume
w	optical mode cross section radius

w_0	optical mode waste radius
x	undulator transverse coordinate parallel to magnetic field
y	undulator transverse coordinate perpendicular to magnetic field
z	undulator longitudinal coordinate
Z_0	Raleigh length
$\tilde{Z}_0$	normalized Rayleigh length
$\vec{\beta}$	non-dimensional electron velocity
$\beta_\perp$	transverse component of
β_z	longitudinal component of
γ	Lorentz factor
δy	magnitude of optical mode shift
$\hat{\varepsilon}_1$	unit vector = $(\cos\psi, -\sin\psi, 0)$
$\hat{\varepsilon}_2$	unit vector = $(-\sin\psi, -\cos\psi, 0)$
ζ	electron phase
η	undulator extraction
θ	mirror tilt
θ_b	electron beam divergence
θ_m	normalized mirror tilt
θ_{y0}	electron beam tilt
$\tilde{\theta}_{y0}$	normalized electron beam tilt
λ	optical wavelength
λ_0	length of undulator period
ν	dimensionless phase velocity
σ	dimensionless electron beam radius
ρ_e	electron density
τ	dimensionless time
ϕ	initial optical phase
ψ	optical phase
ω	optical frequency
ω_0	undulator frequency

LIST OF ACRONYMS

ASCM	Anti-Ship Cruise Missile
CIC	Combat Information Center
CO	Commanding Officer
FEL	Free Electron Laser
FELWS	Free Electron Laser Weapon System
HEL	High Energy Laser
IPS	Integrated Power System
LINAC	Linear Accelerator
NSFS	Naval Surface Fire Support
NSSMS	Nato Seasparrow Missile System
NTDS	Naval Tactical Data System
PSD	Position Sensing Device
PZT	Piezzo Electric Transducer
SLBD	Sea Lite Beam Director
SWC	Ship's Weapon Coordinator
TAO	Tactical Action Officer
TAS	Target Acquisition System
WCC	Weapons Coordinator Console
UAV	Unmanned Aerial Vehicle

THIS PAGE INTENTIONALLY LEFT BLANK

ACKNOWLEDGMENTS

There is no way I could ever properly thank all those who assisted me in this endeavor. After having written many ten to fifteen page reports, I first thought a thesis was nothing more than a collection of those efforts. Boy was I wrong. I'd like to thank Prof. Colson for your time and advice. Your ability to clearly explain the most complex topic has been paramount to my understanding of directed energy.

To Professor Armstead, who always has a smile on his face or a joke for the class. You have always left me with the impression that, regardless of the situation, you've seen it before.

To Professors Blau and Crooker. Thank you for all the advice and taking the time to answer my questions. It helped me not to look quite as foolish in Prof. Colson's office.

To my fellow students in the lab, lights out…its go time!

To my son Sean, watching you grow over the past 27 months has been the highlight of my life. Your hugs and smiles have melted the coldest of my days.

And finally, to my wife Karen. Your support has been unfaltering throughout the past 7 years. I would not be where I am if it wasn't for your selfless sacrifices. I love you.

THIS PAGE INTENTIONALLY LEFT BLANK

I. INTRODUCTION

In the commencement address at the Naval War College given on Jun 20, 2003, Deputy Defense Secretary Paul D. Wolfowitz declared "today's U.S. military leaders need to think outside the box to contend with massive changes occurring in the national security realm…Transformation means profound change." [Wolfowitz] This change includes focusing on the development of "generation after next" weapons so that the U.S. can maintain technological superiority over any threat throughout the globe.

One area of technological superiority the U.S. Navy is exploring is directed energy. With the advent of the "all electric ship" design being implemented on the Navy's next class of destroyer, DD(X), there will be sufficient resources to power electric weapons, such as an electromagnetic railgun or an electric High Energy Laser (HEL). According to PMS 405 Program Manager CAPT Roger McGinnis, the Navy is now focusing the HEL program on Free Electron Lasers (FEL) because they do not suffer the same thermal management problems that solid state lasers do, and they can operate in maritime environments, unlike chemical lasers [Truver].

Advantages of the FEL as a weapon system include supply, tunability, flexibility, and operating cost [Campbell]. An FEL uses electricity as its power source, so as long as the ship has fuel to run its electric generator, the FEL can continue to operate. This gives the FEL a significant advantage over conventional weapons that require reloading and logistical re-supply. Unlike other lasers, FELs are tunable. This permits them to exploit wavelength dependent atmospheric propagation windows. Unlike conventional weapon systems that are tailored to a specific mission area, FELs are flexible. Not only are they useful in anti-ship cruise missile defense; the precision associated with a laser weapon gives them the ability to engage surface contacts without the fear of collateral damage associated with missile or gun systems. Finally, since the fuel for the FEL comes from the ship's electric power, the operating cost of an engagement is the cost of the increased fuel consumption. At current fuel prices, this amounts to about $2 per 5 second engagement.

No weapon system comes without disadvantages, and the FEL is no exception. FELs are large machines. Current designs reduce the projected size to a box approximately 4 meters wide, 4 meters tall, and 16-20 meters long. This size is small enough to be implemented in a new ship design, but most likely too large to be back fitted into existing platforms. Another disadvantage is the initial cost of the FEL. The projected cost of the weapon system is about 50 million dollars. Although initially a very expensive device, the FEL may still be cheaper than conventional weapons over a lifetime because of its very inexpensive operating cost [Ossenfort].

This thesis explores the shipboard employment of a free electron laser weapon system. Chapter II gives a detailed description of a conceptual plan for a ship-borne FEL using a recirculating electron beam configuration, including a description of the principle components of the design.

Chapter III presents the classical theory of a free electron laser using a helical undulator. The electron equations of motion and optical wave equations are developed for a relativistic electron beam. The transfer of energy from the electron to optical beam is then explained through a discussion of gain and electron phase space.

Chapter IV investigates the design considerations of a short Rayleigh length FEL. Results of multimode computer simulations are used to predict effects of mirror stability and optimum design parameters.

Chapter V develops a concept of operations for employing an FEL. Three scenarios are used to discuss the flexibility of the system: anti-ship cruise missile defense, small boat attack, and naval surface fire support.

II. DETAILED DESCRIPTION OF A FREE ELECTRON LASER

A. ELECTRON BEAM

The components of the electron beam apparatus include the injector, accelerator, beam transport system, undulator, and the beam dump. There are two basic configurations of the electron beam components. One is a single-pass configuration in which the beam of free electrons from the accelerator is passed through the undulator once before terminating at the beam dump. The other style is a recirculating configuration where the electrons are returned to the accelerator after passing through the undulator. Figure 1 shows a conceptual plan for a ship-borne free electron laser using the recirculating style configuration.

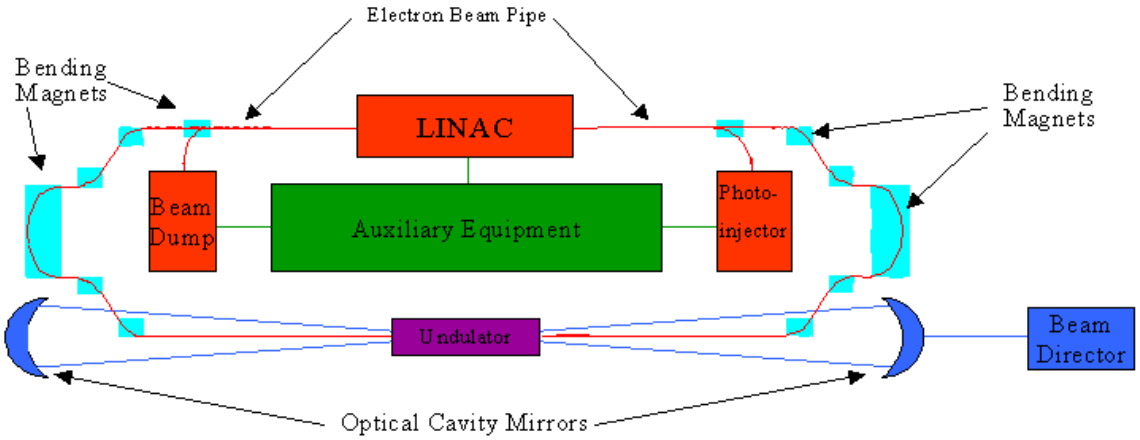

Figure 1 Major Components of a Free Electron Laser. Electron Beam components are shown in red, the optical beam components are shown in blue, and the auxiliary equipment is shown in green. The undulator, shown in purple, is where energy from the electron beam is transferred to the optical beam.

1. Electron Injector

The electron beam originates from an injector. The injector produces free electrons in vacuum either through thermal emission or photoemission from a cathode surface. Either way, the emitted electrons are accelerated via a static or RF electric field at the end of the injector into a stainless steel beam-pipe transport system and on into the accelerator. Electrons in the current laser design will leave the injector with 7 MeV of energy.

2. Electron Accelerator

The electron accelerator increases the energy of the electron beam with an intense electric field stored in radiofrequency (RF) cavities. The frequency of the modules is synchronized with the electron injection frequency so that the electrons are continuously accelerated. In the current design, the electric field is intense enough to provide a 15MeV/m acceleration gradient so that the electrons emerge from the 7 m long accelerator at about 100 MeV.

3. Undulator

The undulator consists of alternating permanent magnets that cause the electrons to "wiggle" back and forth slightly as they pass through the magnetic field in accordance with the Lorentz Force law. As the relativistic electrons oscillate, they radiate light along the axis of the undulator. An optical cavity encloses the undulator and bounces the light back and forth between two mirrors. The reflected optical radiation travels along the undulator axis collinear with subsequently injected electrons, thereby stimulating the new electrons to radiate coherent energy and increase the power of the optical beam. In the current design, the undulator is 37 cm long and has 14 periods; each 2.66 cm in length, and the magnetic field is approximately 1 T.

4. Electron Beam Transport System

The electron beam is "piped" between its components via stainless steel tubing under a virtually perfect vacuum in order to prevent gas molecules from scattering or interacting with the electrons. The recirculating configuration consists of several bends through which the electrons must be steered. This is accomplished by using magnetic fields generated by adjustable magnets to guide the electron beam inside the bend of the tubing.

5. Electron Beam Dump

Even in a recirculating configuration, not all of the energy can be recovered, so a portion of the energy (~7 MeV in this design) terminates in an electron beam dump. The dump consists of a highly electrophilic material, such as copper, which absorbs the high-speed electrons. When the high-speed electrons are absorbed, energy is released in the

form of heat and radiation. The beam dump is externally cooled in order to dissipate the heat and shielded in order to contain the radiation.

B. OPTICAL BEAM

The optical beam apparatus is comprised of the optical beam cavity, the optical beam piping, and the beam director. Optical radiation (light) is stored inside the optical cavity while a fraction of it passes through a partially reflecting mirror located at one end. The light then travels through the ship to the beam director via the optical beam pipe, where it is focused on the target.

1. Optical Cavity

The optical cavity consists of a long cylinder at a near perfect vacuum with a spherical mirror at each end. One of the mirrors is approximately 50% transmissive, allowing a part of the optical radiation to escape the optical beam cavity. The distance between the two mirrors is critical and must be kept constant so that all of the successive passes of the light pulses remain in phase with the sequence of electron pulses. In addition to the separation distance, the alignment of the mirrors is also critical to laser operation. Since the optical and electron radiation must overlap, the focus of the mirrors must coincide with the undulator near the center of the optical cavity. Beam stability is maintained by utilizing an active alignment system that makes small adjustments to the mirrors as needed to keep the separation distance and alignment within tolerance.

a. Resonance

In the undulator, the electrons travel at a velocity slightly less than the speed of the radiated light. Significant optical gain is achieved near resonance when the difference in velocities is sufficient to allow one wavelength of light to pass over the electron as it travels through one period of the undulator. This electron-photon "race" determines the wavelength of the laser. At resonance, a point fixed in the optical wave must travel a distance of $\lambda + \lambda_0$ in the same amount of time required for the electron to travel a distance of λ_0, where λ_0 is the wavelength of the undulator and λ is the

wavelength of the light. Figure 2 shows an electron (red) traveling a distance of one undulator wavelength (green) as one wavelength of light (blue) passes over it.

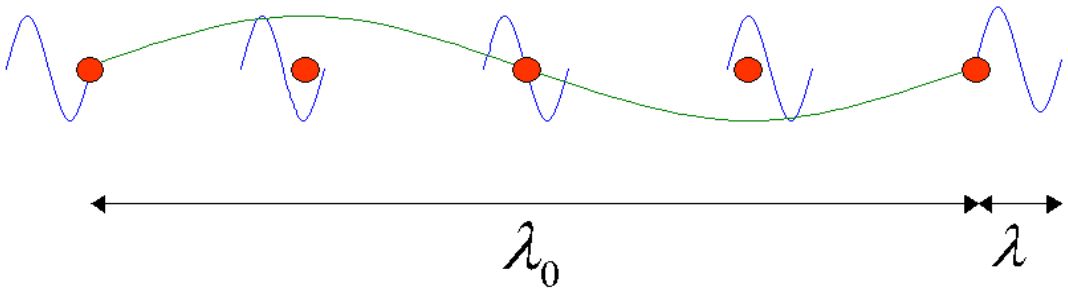

Figure 2 The Electron-Photon Race. One wavelength of light (blue) passes over one electron (red) as the electron travels a distance equal to one undulator period (green).

b. Optical Mirrors

Once the optical beam has been generated, it will be stored between the two mirrors on each end of the optical cavity. Considering a partially reflective (out-coupling) mirror that is approximately 50% transparent, the optical power stored in the resonator will be a few megawatts for a MW class laser. (This is a figure of speech that means the optical power passing any cross-section of the resonator is a few megawatts.) Even with surfaces that are over 99.9% reflective, the absorbed energy would still destroy the mirror if the size of the spot on the mirror were too small. Since the power in the beam remains constant, a larger spot size reduces the power per unit area (intensity) of the beam. Using spherical mirrors that focus the optical beam near the center of the cavity enlarges the spot size. As the beam expands with distance, the energy gets distributed over a larger area and the intensity decreases. Modern cryogenic mirrors are limited to 200 kW/cm^2, so the length of the cavity or the rate of divergence (characterized inversely by the Rayleigh length) must be sufficient to reduce the intensity of the optical beam below this threshold.

c. Stability

In an FEL, the optical and electron pulses must overlap in order to exchange energy, which is accomplished by aligning the mirrors so the optical beam

focuses on the electron beam and by positioning the mirrors so the optical pulses are synchronized with the electron pulses. If the focus of the optical beam is shifted off of the electron beam, the optical pulses miss the electron pulses all together. If the distance between the mirrors or the position of the mirrors with respect to the electron beam changes, then the optical pulses will not overlap the electron pulses. An active feedback alignment system is employed to position and align the mirrors as necessary to maintain stability.

d. Active Alignment

Alignment of the optical system is accomplished via a low powered measuring laser and an active feedback system control system, such as the one shown in Figure 3. Once the mirrors are properly positioned and aligned, they are monitored with a small laser. Any small shift or tilt is identified by a position sensing device (PSD). A control signal is generated by the feedback circuit, amplified by the PZT driver, and is sent to a piezzo electric transducer (PZT) that makes compensating position adjustments to the mirror. Simulations show the required mirror stability is on the order of 100 μrad. [Crooker] Laboratory alignment systems can hold mirrors within 0.1 μrad, which is significantly greater than required.

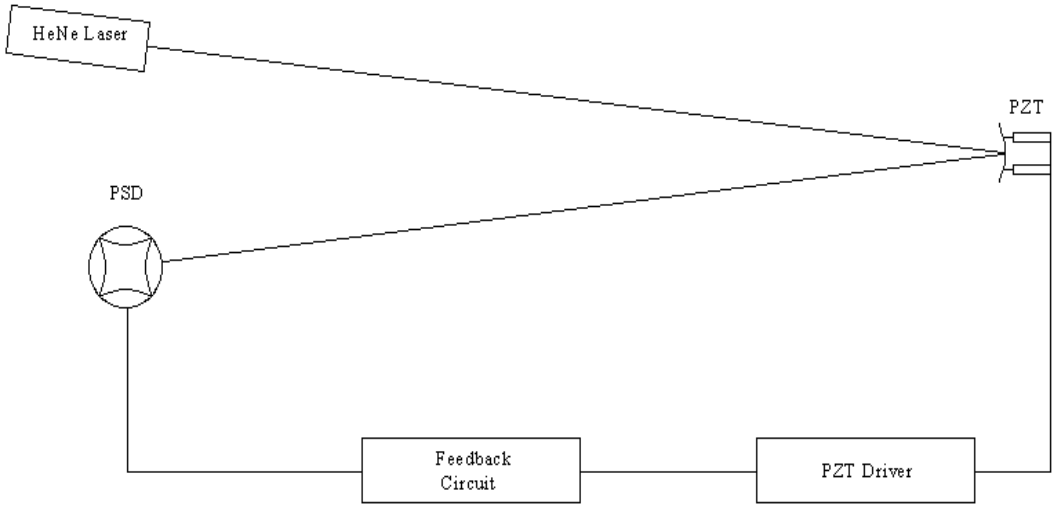

Figure 3 Block Diagram of Jefferson Lab Active Alignment System. From [Behre] Mirror position fluctuations are sensed by the PSD. Feedback circuitry generates positioning signals that are used by the PZT to realign the mirror.

2. Optical Beam Piping

Once the optical beam has been generated it will be guided to the beam director via an optical transport system. The system will consist of a series of straight tubes through which the beam will pass connected by mirrors to change the beam direction. Light coming from the outcoupling mirror will still be diverging and needs to reflect off a collimating mirror before it can propagate to the beam director. The optical system will need to be under vacuum in order to prevent the beam from losing energy due to absorption and scattering.

3. Beam Director

In the free electron laser weapon system, the beam director is where the high power optical beam leaves the ship. Since it the last piece of equipment to interact with the laser, it represents the final opportunity for any modifications to be made to the beam. Additionally, as the final component of the weapon system, it must not only be able to aim the beam on the target, but hold it steady for as long as required to destroy the threat. Beam directors, such as the Sea Lite Beam Director (SLBD), use adaptive optics to make the necessary final adjustments to the beam and inertial stabilization to hold the beam steady on the target.

a. Sea Lite Beam Director

Unlike missile or gun systems, lasers have an advantage because they can be instantly aimed. This also leads to the necessity of tight beam control to prevent the laser from wandering around the target and not delivering the intensity necessary to destroy it. Therefore, beam control entails acquiring and tracking a target as well as keeping the beam fixed on the target for the duration of the engagement. The Sea Lite Beam Director (Figure 4) uses a stabilized line of sight concept to achieve precision pointing and tracking. Optical sensors use an inertially stabilized gimbal reference mirror to detect alignment errors and send position commands to the beam steering mirrors. In turn, the beam steering mirrors can quickly move the beam by not having to move the entire director. This enables rapid and precision pointing of the high power laser.

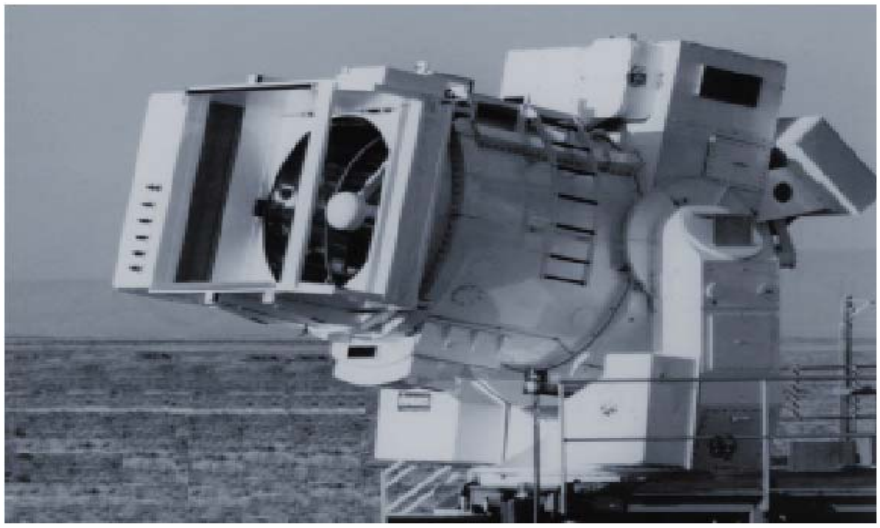

Figure 4 Sea Lite Beam Director (SLBD). From [Pentek] The SLBD is used to acquire and track a target by focusing and holding the laser beam on the moving target long enough to destroy or disable it.

b. Adaptive Optics

Adaptive optics utilize optical beam feedback to make adjustments as needed to the optical wavefront. Not only are adjustments necessary for improving the quality of the beam, but for overcoming negative propagation effects such as turbulence. Turbulence is caused by the inhomogeneous nature of the atmosphere. This non-uniformity acts like several random lenses that distort the propagation path of the beam.

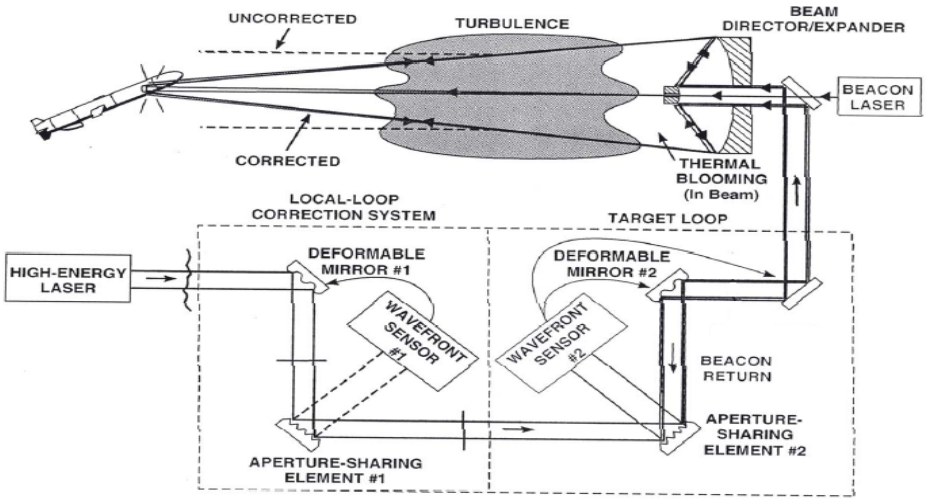

Figure 5 Adaptive Optics. From [Albertine] A local-loop correction system is used to improve beam quality and a target loop is used to correct for atmospheric effects. In each loop, distortions in the phasefront of the optical wave are measured and corrected by deformable mirrors.

Beam directors use an adaptive optics system, such as the one depicted in Figure 5 to improve optical beam quality, as well as to correct for turbulence. Using an aperture-sharing element, the phase front of the optical wave is sampled by a wave front sensor (Figure 6). The wave front sensor uses an array of "lenslets" to divide the optical wave into small beamlets focused onto a detector array. The detector array determines phase front deviations by measuring the local beam tilt of each of the beamlets. The conjugate of the phase front is supplied to a deformable mirror (Figure 7) in order to correct for distortions and improve the beam quality. At the same time, a beacon laser is slaved to the director and focused on the target. Since the beacon laser propagates through the same atmosphere as the high-power beam, it is distorted similarly. Energy reflected off the target is returned to the beam director where a second aperture-sharing element and a second wave front sensor are used to sample the distortions to the beacon laser. This separate feedback loop is used to correct for atmospheric effects.

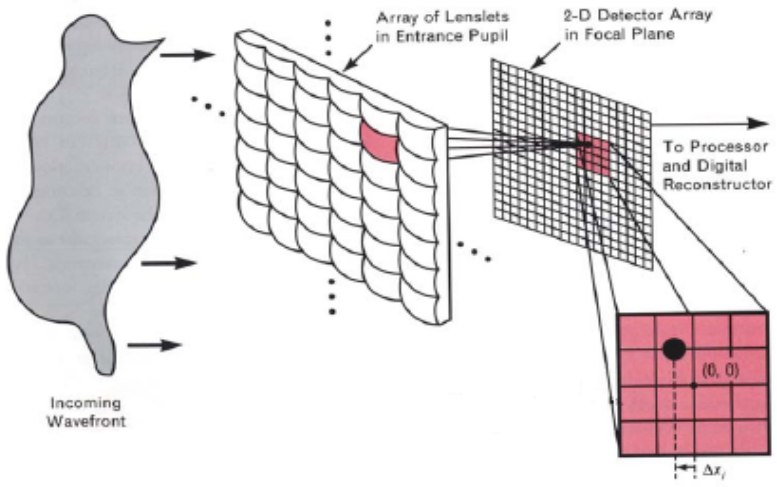

Figure 6 Wavefront Sensing. From [Albertine] A wavefront sensor breaks the optical plane into small beamlets that are then focused by tiny lenslets onto a detector array. Each beamlet has a local beam tilt that is processed by the detector. A correction signal is then generated and used by a deformable mirror to improve the shape of the beamfront.

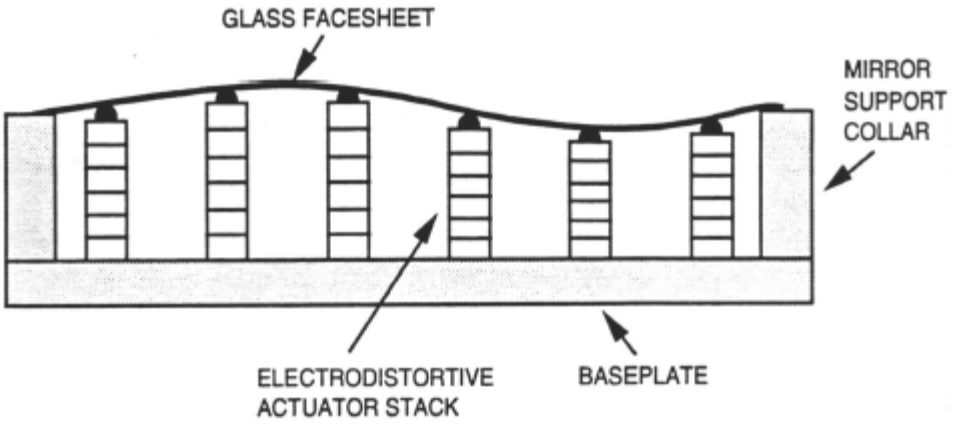

Figure 7 Deformable Mirror. From [Albertine] A deformable mirror consists of a flexible reflective facesheet and a rigid baseplate. Tiny electrodistortive actuator stacks are positioned across the reflective plane. Signals from a wavefront sensor are used to shape the mirror and correct the phasefront of the beam.

C. AUXILLIARY EQUIPMENT

In addition to electron and optical components, FELs require support from auxilliary equipment for operation. These systems include electrical power, refrigeration, radiation shielding, and fresh water cooling.

1. Electrical Power

The electron accelerator and injector require electrical power to increase the energy of the electron beam to 97 MeV. Since the wallplug efficiency for a MW class FEL is estimated to be about ten percent, the total power required will be on the order of 10 MW. Today's ships do not generate that much electrical power and would require energy storage devices, such as capacitors or flywheels, to meet the needs of the system. Future warships plan to include an integrated power system (IPS) of approximately 80MW, which would meet the needs of an FEL system.

2. Refrigeration

The electron generator and accelerator for a MW class FEL will be super-conducting and must operate at temperatures around 2 K. Liquid helium cooling systems are already in use and would be likely candidates for refrigerating the super-conducting

components. The mirrors at the ends of the optical cavity are going to be exposed to megawatts of power and will require a small amount of cooling from the refrigeration system as well.

3. Fresh Water Cooling

A fresh water cooling loop will be required to remove heat from the electronic control systems, the beam dump, and the refrigeration system. Modern ships have similar cooling loops which use cold water to remove the heat from various systems. Thermal energy is transferred to the water, increasing the temperature. The water then passes through a heat exchanger where it is cooled to its original temperature and repeats the cycle. The heat exchanger uses sea water (an unlimited heat sink) to remove the thermal energy from the fresh water cooling loop.

4. Radiation Shielding

In an FEL, the electron injector, the wiggler, the electron transport system, the optical beam, and the beam dump generate radiation. Dense material, such as lead, will be required to shield equipment and personnel from hazardous radiation.

III. FEL THEORY

The combined forces from three fields accelerate electrons propagating through the undulator: the optical magnetic field (B_S), the optical electric field (E_S), and the undulator magnetic field (B_U). Electron acceleration can be described by the relativistic Lorentz force equation

$$\frac{d\left(\gamma\vec{\beta}\right)}{dt} = -\frac{e}{mc}\left(\vec{E}_S + \vec{\beta}\times\vec{B}\right), \tag{3.1}$$

where $\vec{B} = \vec{B}_S + \vec{B}_U$, c is the speed of light, $\vec{v} = \vec{\beta}c$ is the velocity of the electron, e is electron charge in cgs units and m is the electron mass. The Lorentz factor (γ) is defined by

$$\gamma = \frac{1}{\sqrt{1-\beta^2}}. \tag{3.2}$$

Using $E_e = \gamma mc^2$, where E_e is the energy of the electron, a 97 MeV electron travels very close to the speed of light with β = 0.999986 and γ = 190.

For a helical undulator $\vec{\beta}_u$, the corresponding optical electric and magnetic fields are

$$\vec{B}_S = E\left(\sin\psi, \cos\psi, 0\right) \tag{3.3}$$

$$\vec{E}_S = E\left(\cos\psi, -\sin\psi, 0\right) \tag{3.4}$$

$$\vec{B}_U = B\left(\cos\left(k_0 z\right), \sin\left(k_0 z\right), 0\right), \tag{3.5}$$

where B is the magnitude of the undulator magnetic field, E is the magnitude of the optical field in cgs units, z is the longitudinal distance along the undulator, $\psi = kz - \omega t + \phi$, $k = 2\pi/\lambda$ is the optical wavenumber, λ is the optical wavelength, ω is

the optical frequency, and ϕ is the optical phase. The undulator wavenumber is defined as $k_0 = 2\pi / \lambda_0$, where λ_0 is the period of the undulator.

A. RESONANCE

Significant optical gain is achieved near resonance, which occurs when one wavelength of light passes over one electron in one undulator period. If Δt is the time required for one electron to travel one undulator period, the distance λ_0, then it is also the time required for one photon of light to travel the distance $\lambda + \lambda_0$ and

$$\Delta t = \frac{\lambda_0}{v_z} = \frac{\lambda + \lambda_0}{c}, \tag{3.6}$$

where v_z is the velocity component of the electron along the undulator axis. Since the velocity of the electron is $\vec{\beta} c$,

$$\vec{\beta} = \left(\beta_x, \beta_y, \beta_z\right), \tag{3.7}$$

and

$$\beta^2 = \beta_x^2 + \beta_y^2 + \beta_z^2 . \tag{3.8}$$

The velocity component of the electron along the undulator has a magnitude

$$v_z = c\sqrt{\beta^2 - \beta_x^2 - \beta_y^2} . \tag{3.9}$$

Defining the transverse velocity ($\vec{\beta}_\perp$) of the electron as

$$\vec{\beta}_\perp = \left(\beta_x, \beta_y, 0\right), \tag{3.10}$$

the longitudinal speed of the electron is given by

$$v_z = c\sqrt{\beta^2 - \beta_\perp^2} . \tag{3.11}$$

The next section will show

$$\beta_\perp^2 = \frac{K^2}{\gamma^2}, \tag{3.12}$$

where the dimensionless undulator parameter K is defined as

$$K = eB\lambda_0 / 2\pi mc^2, \tag{3.13}$$

and K is of order unity.

Substituting equation (3.11) for v_z in equation (3.6),

$$\frac{\lambda_0}{c\sqrt{\beta^2 - \beta_\perp^2}} = \frac{\lambda + \lambda_0}{c} \tag{3.14}$$

Equation (3.2) can be written as $\beta^2 = 1 - \gamma^{-2}$. Using equations (3.2) and (3.12), equation (3.14) becomes

$$\frac{\lambda_0}{\sqrt{1 - \frac{1+K^2}{\gamma^2}}} = \lambda + \lambda_0 . \tag{3.15}$$

For $\gamma \approx 190 \gg 1$,

$$\sqrt{1 - \frac{1+K^2}{\gamma^2}} \approx 1 - \frac{1+K^2}{2\gamma^2} \tag{3.16}$$

and equation (3.15) becomes

$$\frac{\lambda_0}{1 - \frac{1+K^2}{2\gamma^2}} = \lambda + \lambda_0 . \tag{3.17}$$

Solving for λ, we have

$$\lambda = \lambda_0 \left(\frac{1}{1 - \frac{1+K^2}{2\gamma^2}} - 1 \right) = \frac{\lambda_0 \left(1+K^2\right)}{2\gamma^2} . \tag{3.18}$$

So that the emitted wavelength of light near resonance is given by

$$\lambda \approx \lambda_0 \frac{1+K^2}{2\gamma^2} . \tag{3.19}$$

Since K depends on the magnetic field of the undulator (B_U) and γ depends on the energy of the electron (E_e), equation (3.19) shows the wavelength of light for a given undulator is a function of the undulator magnetic field and the electron energy.

B. ELECTRON MOTION

An electron traveling the length of the undulator will interact with the electrical and optical fields due to the Lorentz Force equation. Substituting equations (3.3), (3.4), and (3.5) into equation (3.1) yields the transverse equations of electron motion

$$\frac{d(\gamma\beta_x)}{dt} = -\frac{e}{mc}\left[E\cos\psi(1-\beta_z) - B\beta_z\sin(k_0 z)\right] \tag{3.20}$$

and

$$\frac{d(\gamma\beta_y)}{dt} = -\frac{e}{mc}\left[-E\sin\psi(1-\beta_z) + B\beta_z\cos(k_0 z)\right]. \tag{3.21}$$

Since the electrons are relativistic $(\gamma \gg 1, \beta_z \approx 1)$, we have, $E(1-\beta_z) \ll B\beta_z$ and equations (3.20) and (3.21) can be simplified into

$$\frac{d(\gamma\beta_x)}{dt} = \frac{eB\beta_z}{mc}\sin(k_0 z) \tag{3.22}$$

and

$$\frac{d(\gamma\beta_y)}{dt} = \frac{-eB\beta_z}{mc}\cos(k_0 z). \tag{3.23}$$

Remembering $\vec{\beta}_\perp = (\beta_x, \beta_y, 0)$ is the transverse velocity, equations (3.22) and (3.23) to be combined into a single equation

$$\frac{d(\gamma\vec{\beta}_\perp)}{dt} = \frac{-eB\beta_z}{mc}\left(-\sin(k_0 z), \cos(k_0 z), 0\right). \tag{3.24}$$

Integrating equation (3.24) results in

$$\gamma\vec{\beta}_\perp = \frac{-eB}{mc^2 k_0}\left(\cos(k_0 z), \sin(k_0 z), 0\right), \tag{3.25}$$

where the constants of integration are set equal to zero by assuming perfect injection into helical orbits. Remembering $k_0 = 2\pi / \lambda_0$, equation (3.25) can be written as

$$\vec{\beta}_\perp = \frac{-eB\lambda_0}{\gamma mc^2 2\pi}\left(\cos(k_0 z), \sin(k_0 z), 0\right). \tag{3.26}$$

Since $K = eB\lambda_0 / 2\pi mc^2$ is the dimensionless undulator parameter, the transverse equation of motion of electrons in a helical undulator becomes

$$\vec{\beta}_\perp = \frac{-K}{\gamma}\left(\cos(k_0 z), \sin(k_0 z), 0\right). \tag{3.27}$$

The transverse velocity magnitude is

$$\beta_\perp^2 = \left(\frac{-K}{\gamma}\right)^2 (\cos^2(k_0 z) + \sin^2(k_0 z)). \tag{3.28}$$

Since $\cos^2(k_0 z) + \sin^2(k_0 z) = 1$, we have

$$\beta_\perp^2 = \frac{K^2}{\gamma^2}, \tag{3.29}$$

so that the derivation of equation (3.12) is completed.

Changes in energy of the relativistic electrons interacting with an optical electric field are described by

$$\frac{d\gamma}{dt} = -\frac{e}{mc}\vec{\beta} \cdot \vec{E}_S. \tag{3.30}$$

Substituting equation (3.4) into equation (3.30) gives

$$\frac{d\gamma}{dt} = -\frac{eE}{mc}\left(\beta_x, \beta_y, \beta_z\right) \cdot \left(\cos\psi, -\sin\psi, 0\right). \tag{3.31}$$

Since $\beta_z \cdot 0 = 0$, β_z does not contribute and equation (3.31) can be written as

$$\frac{d\gamma}{dt} = -\frac{eE}{mc}\vec{\beta}_\perp \cdot \left(\cos\psi, -\sin\psi, 0\right). \tag{3.32}$$

Substituting equation (3.27) for $\vec{\beta}_{\perp}$, equation (3.32) becomes

$$\frac{d\gamma}{dt} = \frac{eEK}{mc\gamma}(\cos(k_0 z)\cos\psi - \sin(k_0 z)\sin\psi). \tag{3.33}$$

Using the trigonometric identity $\cos(A+B) = \cos A\cos B - \sin A\sin B$, equation (3.33) can be written as

$$\frac{d\gamma}{dt} = \frac{eEK}{mc\gamma}\cos((k_0 z)+\psi). \tag{3.34}$$

Remembering $\psi = kz - \omega t + \phi$, the energy exchange equation becomes

$$\frac{d\gamma}{dt} = \dot{\gamma} = \frac{eEK}{mc\gamma}\cos(\zeta + \phi), \tag{3.35}$$

where $\zeta = (k + k_0)z - \omega t$ is defined as the electron phase.

Using equations (3.8) and (3.10), equation (3.2) can be written as

$$\beta_{\perp}^2 + \beta_z^2 = 1 - \gamma^{-2}. \tag{3.36}$$

Using equation (3.29), the above equation can be written as

$$1 - \beta_z^2 = \frac{1+K^2}{\gamma^2}. \tag{3.37}$$

Taking the time derivative of equation (3.37) yields

$$-2\beta_z\dot{\beta}_z = -2\dot{\gamma}\frac{1+K^2}{\gamma^3}, \tag{3.38}$$

which can be rearranged into

$$\frac{\dot{\gamma}}{\gamma} = \frac{\gamma^2\beta_z\dot{\beta}_z}{1+K^2}. \tag{3.39}$$

The second time derivative of the electron phase (ζ) is

$$\ddot{\zeta} = (k + k_0)c\dot{\beta}_z. \tag{3.40}$$

Solving for $\dot{\beta}_z$ and substituting into equation (3.39) yields

$$\frac{\dot{\gamma}}{\gamma} = \frac{\gamma^2 \beta_z \ddot{\zeta}}{(1+K^2)(k+k_0)c} \tag{3.41}$$

From equation (3.19), the resonance condition can be written as

$$\frac{\gamma^2}{1+K^2} = \frac{\lambda_0}{2\lambda}. \tag{3.42}$$

Substituting equation (3.42) into equation (3.41), we have

$$\frac{\dot{\gamma}}{\gamma} = \frac{\lambda_0 \beta_z \ddot{\zeta}}{2\lambda(k+k_0)c}. \tag{3.43}$$

Since $\gamma \gg K$, $\lambda \ll \lambda_0$ and $k \gg k_0$, we have $c(k+k_0) \approx kc = \omega$. Equation (3.43) can be approximately written as

$$\frac{\dot{\gamma}}{\gamma} \approx \frac{\lambda_0 \beta_z \ddot{\zeta}}{2\lambda\omega}. \tag{3.44}$$

Considering $\omega = kc$ and $\omega_0 = k_0 c$, we have

$$\omega / k = \omega_0 / k_0. \tag{3.45}$$

The optical wavenumbers $k = 2\pi/\lambda$ and $k_0 = 2\pi/\lambda_0$ permit the above equation to be written as

$$\frac{\omega}{2\pi/\lambda} = \frac{\omega_0}{2\pi/\lambda_0}, \tag{3.46}$$

which leads to $\omega_0 = \omega\lambda/\lambda_0$ and equation (3.44) becomes

$$\frac{\dot{\gamma}}{\gamma} = \frac{\beta_z \ddot{\zeta}}{2\omega_0}. \tag{3.47}$$

Combining equations (3.35) and (3.47), we have

$$\frac{\ddot{\zeta}\gamma}{2\omega_0} = \frac{eKE}{\gamma mc}\cos(\zeta+\phi), \tag{3.48}$$

where β_z has been set equal to one to be consistent with previous approximations. Equation (3.48) can now be written as

$$\ddot{\zeta} = \frac{2\omega_0 eKE}{\gamma^2 mc}\cos(\zeta + \phi). \tag{3.49}$$

Equation (3.49) shows electrons traveling the length of the undulator experience longitudinal dynamics described by the simple pendulum equation.

A convenient method of generalizing pendulum dynamics is though the use of dimensionless variables. Dimensionless time, τ, goes from zero to one as the relativistic electron $(\beta_z \approx 1)$ passes from the beginning to the end of the undulator and is defined by

$$\tau = \frac{\beta_z ct}{L} \approx \frac{ct}{L}, \tag{3.50}$$

where L is the length of the undulator. Thus,

$$\frac{d}{dt} = \frac{d\tau}{dt}\frac{d}{d\tau} = \frac{c}{L}\frac{d}{d\tau}. \tag{3.51}$$

Using equation (3.51), the pendulum equation can be written as a second-order differential equation with respect to dimensionless time,

$$\ddot{\zeta} = \frac{d^2\zeta}{dt^2} = \frac{c^2}{L^2}\frac{d^2\zeta}{d\tau^2} = \frac{c^2}{L^2}\overset{\circ\circ}{\zeta}, \tag{3.52}$$

so that equation (3.49) becomes

$$\overset{\circ\circ}{\zeta} = \frac{2\omega_0 eKE}{\gamma^2 mc}\left(\frac{L^2}{c^2}\right)\cos(\zeta + \phi), \tag{3.53}$$

where the symbol $\overset{\circ\circ}{\zeta}$ represent the second dimensionless time derivative of ζ. The length of the undulator can be expressed as

$$L = N\lambda_0, \tag{3.54}$$

where N is the number of periods in the undulator. Substituting for L and remembering $\omega_0 = (2\pi/\lambda_0)c$, the pendulum equation can be expressed as

$$\overset{\circ\circ}{\zeta} = |a|\cos(\zeta + \phi), \tag{3.55}$$

where

$$|a| \equiv \frac{4\pi NeKEL}{\gamma^2 mc^2}. \tag{3.56}$$

The dimensionless electron phase velocity is defined as

$$\nu = \overset{\circ}{\zeta} = L\left[(k + k_0)\beta_z - k\right] \tag{3.57}$$

where $\overset{\circ}{\zeta}$ is the first dimensionless time derivative of ζ.

Equation (3.55) shows how electrons traveling through the undulator evolve as they are driven by an optical field with an amplitude of $|a|$. When the dimensionless electron phase velocity, ν, is zero, equation (3.57) shows the electron velocity is $\beta_z = k/(k + k_0)$ and is at resonance. When $\beta_z > k/(k + k_0)$, ν is positive and when $\beta_z < k/(k + k_0)$, ν is negative. Changes in the electron phase velocity are due to energy exchanges with the optical field. A loss of energy from the optical field results in an increase in ν while a decrease in ν indicates an increase of energy in the optical field. Since the goal of the FEL is to transfer electron energy into light, a net reduction in ν is desirable.

C. OPTICAL WAVE EQUATION

The previous section examined the effect of the optical field on an electron traveling the length of the undulator. This section will develop how electron propagation affects the optical field. The propagation of the optical wave can be described by the wave equation in cgs units

$$\left(\nabla^2 - \frac{1}{c^2}\frac{\partial^2}{\partial t^2}\right)\vec{A} = -\frac{4\pi}{c}\vec{J}_\perp, \tag{3.58}$$

where $\vec{A}$ is the optical vector potential and $\vec{J}_\perp$ is the transverse current density. Since the vector potential is defined as

$$\vec{B}_S = \vec{\nabla} \times \vec{A}, \tag{3.59}$$

the vector potential can be found using equation (3.3) to be

$$\vec{A} = \frac{E}{k}\left(\sin\psi, \cos\psi, 0\right). \tag{3.60}$$

The second spatial and time derivatives are

$$\begin{aligned} \nabla^2 \vec{A} = & \left[\frac{1}{k}\frac{\partial^2 E}{\partial z^2} - \frac{E}{k}\left(k + \frac{\partial \phi}{\partial z}\right)^2\right]\left(\sin\psi, \cos\psi, 0\right) \\ & + \left[\frac{2}{k}\frac{\partial E}{\partial z}\left(k + \frac{\partial \phi}{\partial z}\right) + \frac{E}{k}\frac{\partial^2 \phi}{\partial z^2}\right]\left(\cos\psi, -\sin\psi, 0\right) \end{aligned} \tag{3.61}$$

and

$$\begin{aligned} \frac{\partial^2 \vec{A}}{\partial t^2} = & \left[\frac{1}{k}\frac{\partial^2 E}{\partial t^2} - \frac{E}{k}\left(\frac{\partial \phi}{\partial t} - \omega\right)^2\right]\left(\sin\psi, \cos\psi, 0\right) \\ & + \left[\frac{2}{k}\frac{\partial E}{\partial t}\left(\frac{\partial \phi}{\partial t} - \omega\right) + \frac{E}{k}\frac{\partial^2 \phi}{\partial t^2}\right]\left(\cos\psi, -\sin\psi, 0\right). \end{aligned} \tag{3.62}$$

For a slowly varying optical phase and amplitude, the second-order and quadratic first order derivatives are small compared to ω and k. Neglecting $\partial^2 E/\partial z^2$, $\partial^2 \phi/\partial z^2$, $\partial \phi^2/\partial z^2$, $\partial E \partial \phi/\partial z^2$, $\partial^2 E/\partial t^2$, $\partial^2 \phi/\partial t^2$, $\partial \phi^2/\partial t^2$, and $\partial E \partial \phi/\partial t^2$ permits equations (3.61) and (3.62) to be written approximately as

$$\nabla^2 \vec{A} \approx 2\frac{\partial E}{\partial z}\left(\cos\psi, -\sin\psi, 0\right) - E\left(k + 2\frac{\partial \phi}{\partial z}\right)\left(\sin\psi, \cos\psi, 0\right) \tag{3.63}$$

and

$$\frac{\partial^2 \vec{A}}{\partial t^2} \approx -\frac{2\omega}{k}\frac{\partial E}{\partial t}\left(\cos\psi, -\sin\psi, 0\right) + \frac{E}{k}\left(2\omega\frac{\partial \phi}{\partial t} - \omega^2\right)\left(\sin\psi, \cos\psi, 0\right) \tag{3.64}$$

keeping only constant terms ω and k, and derivatives of E and ϕ. Substituting equations (3.63) and (3.64) into equation (3.58), the optical wave equation becomes

$$2\left(\frac{\partial E}{\partial z} + \frac{1}{c}\frac{\partial E}{\partial t}\right)\left(\cos\psi, -\sin\psi, 0\right) - 2E\left(\frac{\partial \phi}{\partial z} + \frac{1}{c}\frac{\partial \phi}{\partial t}\right)\left(\sin\psi, \cos\psi, 0\right) = -\frac{4\pi}{c}\vec{J}_\perp \tag{3.65}$$

The spatial coordinate z^* is used to represent a point that follows the light and is defined as

$$z^* = z - ct. \tag{3.66}$$

By rewriting equation (3.50) as $t = L\tau / c$, equation (3.66) becomes

$$z^* = z - L\tau. \tag{3.67}$$

This change in coordinates leads to the following changes in the operators $\partial / \partial z$ and $\partial / \partial t$:

$$\frac{\partial}{\partial z} = \frac{\partial z^*}{\partial z}\frac{\partial}{\partial z^*} + \frac{\partial \tau}{\partial z}\frac{\partial}{\partial \tau} \tag{3.68}$$

and

$$\frac{\partial}{\partial t} = \frac{\partial z^*}{\partial t}\frac{\partial}{\partial z^*} + \frac{\partial \tau}{\partial t}\frac{\partial}{\partial \tau}. \tag{3.69}$$

Using equations (3.50) and (3.67), $\partial z^* / \partial z = 1$, $\partial z^* / \partial t = -c$, $\partial \tau / \partial z = 0$, and $\partial \tau / \partial t = c / L$. Equations (3.68) and (3.69) become

$$\frac{\partial}{\partial z} = \frac{\partial}{\partial z^*} \tag{3.70}$$

and

$$\frac{\partial}{\partial t} = -c\frac{\partial}{\partial z^*} + \frac{c}{L}\frac{\partial}{\partial \tau}. \tag{3.71}$$

Using equations (3.70) and (3.71), the operator becomes

$$\frac{\partial}{\partial z} + \frac{1}{c}\frac{\partial}{\partial t} = \frac{\partial}{\partial z^*} + \frac{1}{c}\left[-c\frac{\partial}{\partial z^*} + \frac{c}{L}\frac{\partial}{\partial \tau}\right] = \frac{1}{L}\frac{\partial}{\partial \tau}. \tag{3.72}$$

Equation (3.65) can be written as

$$\frac{2}{L}\frac{\partial E}{\partial \tau}(\cos\psi, -\sin\psi, 0) - \frac{2E}{L}\frac{\partial \phi}{\partial \tau}(\sin\psi, \cos\psi, 0) = -\frac{4\pi}{c}\vec{J}_{\perp}. \tag{3.73}$$

Defining unit vectors $\hat{\varepsilon}_1 = (\cos\psi, -\sin\psi, 0)$ and $\hat{\varepsilon}_2 = (-\sin\psi, -\cos\psi, 0)$ and forming the inner product with equation (3.73) and $\hat{\varepsilon}_1$ and $\hat{\varepsilon}_2$ in turn permits the above equations to be decoupled into

$$\frac{\partial E}{\partial t} = -\frac{2\pi L}{c}\vec{J}_\perp \cdot \hat{\varepsilon}_1 \tag{3.74}$$

and

$$E\frac{\partial \phi}{\partial t} = -\frac{2\pi L}{c}\vec{J}_\perp \cdot \hat{\varepsilon}_2 . \tag{3.75}$$

The transverse current $\vec{J}_\perp$ can be written as the sum of the individual electron currents

$$\vec{J}_\perp = \sum_i \left[-ec\vec{\beta}_\perp \delta^3(\vec{x} - \vec{r}_i) \right], \tag{3.76}$$

where δ^3 is the three dimensional Dirac delta function and $\vec{r}_i$ is the position of the i^{th} electron. Substituting equation (3.27) into equation (3.76), the transverse current becomes

$$\vec{J}_\perp = \frac{Kec}{\gamma}\sum_i \delta^3(\vec{x} - \vec{r}_i)\left(\cos(k_0 z), \sin(k_0 z), 0\right). \tag{3.77}$$

Equations (3.74) and (3.75) can be written as

$$\frac{\partial E}{\partial \tau} = \frac{-2\pi KeL}{\gamma}\sum_i \delta^3(\vec{x} - \vec{r}_i)\left[\cos(k_0 z)\cos\psi - \sin(k_0 z)\sin\psi\right], \tag{3.78}$$

and

$$E\frac{\partial \phi}{\partial \tau} = \frac{2\pi KeL}{\gamma}\sum_i \delta^3(\vec{x} - \vec{r}_i)\left[\cos(k_0 z)\sin\psi + \sin(k_0 z)\cos\psi\right]. \tag{3.79}$$

A volume element of electrons with number density ρ_e times the average od sampled electron phase can be used to replace the sum of all the individual electron phases. The trigonometric identities $\cos(A+B) = \cos A\cos B - \sin A\sin B$ and $\sin(A+B) = \sin A\cos B + \cos A\sin B$ transforms the above equations into

$$\frac{\partial E}{\partial \tau} = \frac{-2\pi KeL\rho_e}{\gamma}\left\langle \cos(\zeta + \phi)\right\rangle, \tag{3.80}$$

and

$$E\frac{\partial \phi}{\partial \tau} = \frac{2\pi KeL\rho_e}{\gamma}\left\langle \sin(\zeta + \phi)\right\rangle, \tag{3.81}$$

where <…> indicates an average over all the sampled electrons. Multiplying equation (3.81) by i and adding it to equation (3.80) yields,

$$\frac{\partial E}{\partial \tau} + iE\frac{\partial \phi}{\partial \tau} = \frac{-2\pi KeL\rho_e}{\gamma}\left\langle \cos(\zeta + \phi) - i\sin(\zeta + \phi)\right\rangle. \tag{3.82}$$

Using phasor notation, the above equation can be written as

$$\frac{\partial E}{\partial \tau} + iE\frac{\partial \phi}{\partial \tau} = \frac{-2\pi KeL\rho_e}{\gamma}\left\langle e^{-i(\zeta+\phi)}\right\rangle. \tag{3.83}$$

Multiplying both sides by $e^{i\phi}$ and using the product rule, we have

$$\frac{\partial Ee^{i\phi}}{\partial \tau} = \frac{-2\pi KeL\rho_e}{\gamma}\left\langle e^{-i\zeta}\right\rangle. \tag{3.84}$$

From equation (3.56),

$$\frac{|a|\gamma^2 mc^2}{4\pi NeKEL} = 1. \tag{3.85}$$

Multiplying the left hand side of equation (3.84) by the above expression yields

$$\frac{\partial}{\partial \tau}\left(\frac{|a|\gamma^2 mc^2 e^{i\phi}}{4\pi NeKL}\right) = \frac{-2\pi KeL\rho_e}{\gamma}\left\langle e^{-i\zeta}\right\rangle, \tag{3.86}$$

which can be written as

$$\frac{\partial a}{\partial \tau} = \frac{-8\pi^2 K^2 e^2 L^2 N\rho_e}{\gamma^3 mc^2}\left\langle e^{-i\zeta}\right\rangle, \tag{3.87}$$

where $a = |a|e^{i\phi}$ is the complex amplitude of the dimensionless optical field. Defining the dimensionless current j as

$$j = \frac{8\pi^2 K^2 e^2 L^2 N \rho_e}{\gamma^3 mc^2} \tag{3.88}$$

permits equation (3.87) to be written in the dimensionless form

$$\overset{\circ}{a} = -j\left\langle e^{-i\zeta} \right\rangle . \tag{3.89}$$

The dimensionless wave equation above shows that changes to the optical field are dependent on the electron beam current and the average phase of the electrons. If the electrons are randomly distributed, then the average phase is near zero and there is no change in the optical field. Only when the electron phases are bunched in phase ζ will the optical field experience changes, gain or loss.

D. GAIN

Gain is defined as the fractional increase of the optical field energy per pass through the undulator. If the gain is above threshold (above the cavity losses), then the FEL can reach high power over many passes. The gain of the FEL, G, is defined as

$$G = \frac{a_1^2 - a_0^2}{a_0^2}, \tag{3.90}$$

where a_0 is the initial dimensionless amplitude of the optical field at beginning of the undulator $(\tau = 0)$ and a_1 is the dimensionless amplitude of the optical field at the end of the undulator $(\tau = 1)$. In each pass, energy is transferred between the electron beam to the optical field, allowing the gain to be determined by calculating the energy loss of the electrons.

The electron energy is proportional to the electron phase velocity given in equation (3.57) as $\nu = L\left[(k + k_0)\beta_z - k\right]$. Since $k >> k_0$, $k + k_0 \approx k$ and the change in the electron phase velocity is given approximately by

$$\Delta\nu \approx Lk\Delta\beta_z . \tag{3.91}$$

Using resonance condition, equation (3.19), and $k = 2\pi / \lambda$, the optical wavenumber can be written as $k = 4\pi\gamma^2 /(1+K^2)\lambda_0$. By substituting into equation (3.91), the change in the electron phase velocity becomes

$$\Delta\nu = \frac{L4\pi\gamma^2\Delta\beta_z}{\lambda_0(1+K^2)}. \tag{3.92}$$

Rewriting equation (3.54) as $N = L/\lambda_0$ permits the above equation to be written as

$$\Delta\nu = \frac{4\pi N\gamma^2\Delta\beta_z}{(1+K^2)}. \tag{3.93}$$

Using equation (3.39), the relationship between $\Delta\beta_z$ and $\Delta\gamma$ can be found to be

$$\Delta\beta_z = \frac{1+K^2}{\gamma^3\beta_z}\Delta\gamma. \tag{3.94}$$

Substituting for $\Delta\beta_z$ in equation (3.93) yields

$$\Delta\nu = 4\pi N\frac{\Delta\gamma}{\gamma}, \tag{3.95}$$

where $\beta_z \approx 1$ for relativistic electrons. Defining the electron energy as $E_e = \gamma mc^2$, the change in the electron energy (ΔE_e) is given by

$$\Delta E_e = mc^2\Delta\gamma \tag{3.96}$$

Solving equation (3.95) for $\Delta\gamma$ and substituting into equation (3.96) yields

$$\Delta E_e = \frac{\gamma mc^2}{4\pi N}\Delta\nu, \tag{3.97}$$

which is the change in the energy of one electron. The total change in the energy of a beam of electrons is given by multiplying equation (3.97) by the total number of electrons contained by a volume element of the optical beam. The number of electrons N_e in a given volume V of the optical beam is given by

$$N_e = \rho_e FV, \tag{3.98}$$

where F is a filling factor defined by the ratio of the cross-sectional areas of the electron and optical beams. Assuming the electron density is constant over a small volume element dV, the number of electrons dN_e in the volume element is given by

$$dN_e = \rho_e F dV . \tag{3.99}$$

Combining equations (3.97) and (3.99), the change in the electron beam energy dE_b within the small volume dV is given by

$$dE_b = \overline{\Delta E_e} dN_e = \frac{\gamma mc^2 \rho_e F}{4\pi N} \overline{\Delta \nu} dV , \tag{3.100}$$

where $\overline{\Delta E_e}$ is the average energy change of an electron and $\overline{\Delta \nu}$ is the average change of the phase velocity in the beam.

The optical field gain can be determined by

$$G = -\frac{dE_b}{dE_o} . \tag{3.101}$$

Since the initial energy content of the optical beam in dV is [Jackson]

$$dE_o = \frac{E^2}{4\pi} dV , \tag{3.102}$$

the gain of the FEL is then

$$G = -\frac{\gamma \rho_e mc^2 F}{NE^2} \overline{\Delta \nu} . \tag{3.103}$$

From equations (3.56) and (3.88),

$$\frac{j}{a_0^2} = \frac{\gamma \rho_e mc^2}{2NE^2} . \tag{3.104}$$

Substituting the above equation into equation (3.103) allows the gain equation to be reduced to

$$G = -\frac{2jF}{a_0^2} \overline{\Delta \nu} . \tag{3.105}$$

Equation (3.105) shows for a given electron current and initial optical field amplitude a_0, the gain of the FEL depends on the average change in the dimensionless electron phase velocity. Electrons that increase in phase velocity remove energy from the optical field (decreasing the gain) while electrons that decrease in phase velocity contribute energy to the optical field (increasing the gain). So long as there is a net decrease in phase velocity, the laser will have positive gain per pass. The overall change in phase velocity is best seen in a phase space plot.

E. PHASE SPACE

The electron's microscopic evolution is described by the pendulum equation

$$\ddot{\zeta} = \dot{\nu} = |a| \cos(\zeta + \phi) . \tag{3.106}$$

Simple pendulum dynamics are often described by using phase space where the angular velocity is plotted as a function of angular position. Likewise, phase space can be useful when examining electron motion in an FEL undulator. Figure 8 shows the evolution of 20 electrons as they travel the length of the undulator (depicted by the progression of the color from yellow to red). The horizontal axis represents dimensionless electron phases and the vertical axis represents dimensionless phase velocity ν_0. The entire coordinate

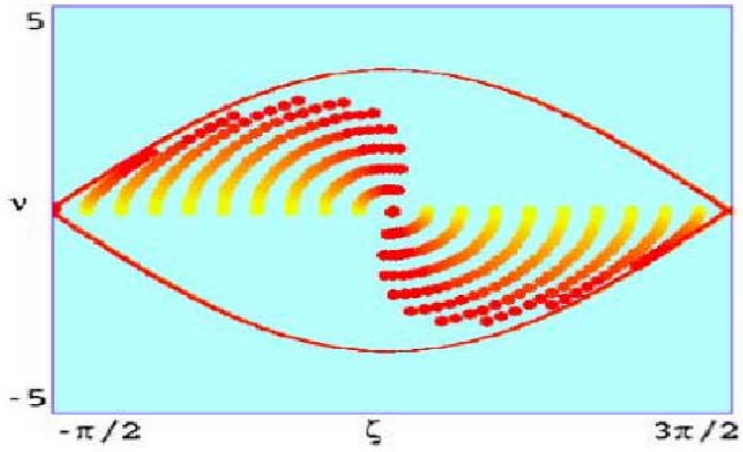

Figure 8 Resonance Phase Space Plot**.** Twenty sample electrons in an FEL distributed along one optical period. The transition from yellow to red depicts the evolution of the electrons as they travel the length of the undulator. Initial phase velocity (ν_0) is equal to zero (resonance).

system represents a section of the electron beam one optical wavelength long. The initial electron phase velocity for the beam is ν_0. Initially, the phases of the electrons are uniformly distributed from $-\pi/2$ to $3\pi/2$ and the initial phase velocity is zero. The 20 electrons represent a sampling of about $\sim 10^6$ randomly distributed electrons in the beam in the same section of phase space. The beam is considered monoenergetic so there is no spread in ν_0. After traveling the length of the undulator, the phase velocity has

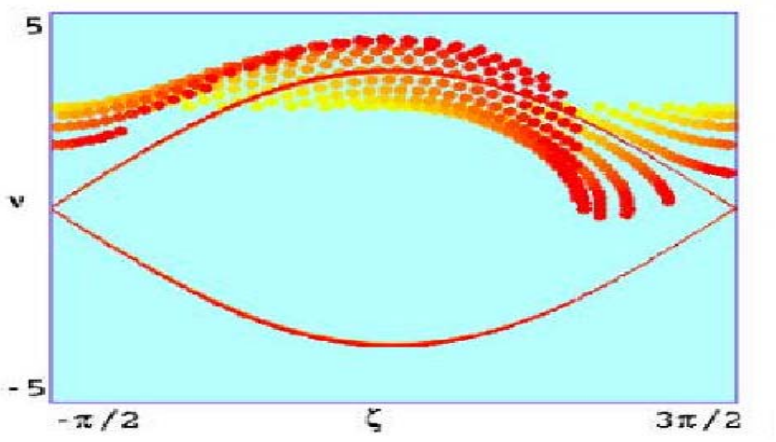

Figure 9 Off Resonance Phase Space**.** Twenty electrons in an FEL with initial phase velocity $\nu_0 = 2.6$. The strong electron phase bunching and net decrease in phase velocity leads to optical field gain.

increased for nine of the electrons, decreased for nine other electrons, and is unchanged for two electrons, one at $\zeta_0 = \pi/2$ and the other $\zeta_0 = -\pi/2$. These are the unstable and stable fixed points in the pendulum phase space. The net change in the phase velocity of all of the electrons is zero, resulting in no gain. In order for an FEL to exhibit gain, the electrons must have an initial phase velocity slightly off resonance.

Figure 9 shows an example of the phase space plot with electrons that have an initial electron phase velocity of $\nu_0 = 2.6$. In this example, electron bunching also occurs, but there is a net decrease in average electron phase velocity. As a result, the optical field experiences positive gain and receives energy from the electron beam.

In an actual free electron laser, the initial phase velocities will not be a single value, but range of values because the beam is not monoenergetic. Typically, the FEL is designed so that this initial spread in ν_0 is not large enough to significantly degrade performance.

THIS PAGE INTENTIONALLY LEFT BLANK

IV. DESIGN CONSIDERATIONS

Although the fundamental physical principles will not change, a free electron laser weapon system will be significantly different than current weapon systems. As with any shipboard system, determining the final design is a multi-faceted process, balanced between experiment and expense. If resources were unlimited, multiple laser systems, each with unique design parameters, could be built and evaluated. The results of these evaluations would demonstrate real operational limitations and eventually lead to an optimum design. However, resources are not unlimited and building many different FELs just to determine the design criteria is impractical. Fortunately, modern computing power permits programs to simulate the complexity of the FEL. Computer simulations performed by the Naval Postgraduate School's Directed Energy and Electric Weapons Center model the evolution of the optical beam as it passes through the undulator. These models provide the ability to alter one or more of the parameters of the FEL in order to find an optimal set of design parameters.

A. SIMULATION METHODS

The program used to model the FEL simulates the evolution of the optical beam during successive passes through the undulator. Parameters that describe the initial conditions of the electron and optical beams, relative orientation of both beams, and geometry of the optical cavity can all be varied in order to study their impact on the operation of the FEL. Typically, only one parameter is varied at a time to gain an appreciation of its effects. Simulations were run for enough passes of light through the undulator for the laser to reach steady state (where the gain of the optical beam equals the losses). After completing each simulation, the energy extraction was recorded and used to determine the output power. Extraction (η) is the amount of energy transferred from the electron beam to the optical beam during one pass through the undulator divided by the electron beam energy, given by

$$\eta = \frac{\langle E_0 - E(z) \rangle}{E_0}, \tag{4.1}$$

where E_0 is the initial electron beam energy and $E(z)$ is the electron beam energy at position z along the length of the undulator. Since $E = \gamma mc^2$, equation (4.1) can be written as

$$\eta = \frac{\langle \gamma_0 - \gamma(z) \rangle}{\gamma_0} \tag{4.2}$$

where γ_0 and $\gamma(z)$ are the respective Lorentz factors at the beginning and position z of the undulator.

Both single-mode and multi-mode simulations were conducted while studying each parameter. In the single mode simulations, the transverse motion of the electron beam was evaluated using an optical mode with determined amplitude and phase. Numerical integrations were performed in order to find the energy exchange and electron phase evolution. From the energy exchange, the extraction was determined. In multi-mode simulations, the three-dimensional evolution of the optical mode was determined in (x,y,t) in accordance with the self-consistent FEL electron and wave equations. This method allows multiple transverse optical modes by breaking the mode into small grid points along the x-y plane, and then allowing the amplitude and phase of each grid point was allowed to evolve independently. Multi-mode simulations are a more accurate model of the physical FEL dynamics, but require hours to perform. On the other hand, the single-mode simulations require seconds to run, so they are used to determine the range each parameter will be varied. Multi-mode simulations are then used to find the effect of each parameter on system performance. Unless otherwise mentioned, multi-mode simulation results will be used throughout the remainder of this thesis.

B. STABILITY

One of the primary challenges of designing a free electron laser weapon system for shipboard use is making it small enough to fit inside a ship. The laser beam expands with distance, so a design with the resonator mirrors close together results in a smaller spot size. This leads to an increase in the intensity of the optical beam on the resonator mirrors. A proposed solution is to utilize a short Rayleigh length design. Since the

Rayleigh length (Z_0) is the characteristic distance in which the cross sectional area of the optical beam increases, a short Rayleigh length design would have a rapidly expanding spot size, given by

$$w^2(z) = w_0^2\left[1+\left(\frac{\lambda z}{\pi w_0^2}\right)^2\right] = w_0^2\left[1+\left(\frac{z}{Z_0}\right)^2\right], \qquad (4.3)$$

where w_0 is the waist radius of the optical mode and $w(z)$ is the waist radius at position z. This increase in area will lower the intensity on the mirrors and permit the separation distance of the resonator mirrors to be short enough to fit inside a ship.

As previously mentioned, FEL operation requires interaction between the electron and optical beams, so the system alignment is crucial. A short Rayleigh length design strongly focuses the optical beam and decreases the interaction region between the two beams. Small perturbations due to shipboard vibrations could potentially lead to a disruption in the stability of the FEL. As with any naval system, anti-shock mounting would be utilized to minimize vibration effects. Furthermore, active alignment would further mitigate vibration effects. However, it would be unrealistic to expect all vibrations to be isolated, so the vibration tolerances of a short Rayleigh length design were investigated.

In our study [Blau] misalignments due to relative tilts of undulator components were investigated using computer simulations. It takes less than one microsecond for photons in a resonator cavity with mirrors spaced between ten and twenty meters apart to complete one period, so the frequency of oscillation is on the order of a megahertz. On the other hand, shipboard vibrations typically occur with frequencies on the order of a kilohertz. Since the photons are moving about three orders of magnitude faster than the system is vibrating, misalignments will appear to be stationary in a photon's frame of reference. For this reason, positional deviations were assumed to be stationary when simulating the performance of the FEL.

1. Electron Beam Tilt

One source of misalignment studied was tilting due to a rotation of the electron beam with respect to the undulator. In this study, the electron beam was incrementally tilted about the beginning and center of the undulator (denoted by $\tau_\beta = 0$ or $\tau_\beta = 0.5$, respectively). The magnitude of tilt was denoted by the parameter $\tilde{\theta}_{y0}$, normalized to the length of the undulator and the wavelength by

$$\tilde{\theta}_{y0} = \theta_{y0}\left(\frac{\lambda}{\pi L}\right)^{-1/2}, \tag{4.4}$$

where θ_{y0} was the tilt in radians.

Figure 10 shows the relative orientation of the electron beam when it ispp tilted about the center of the undulator. In this figure, the electron beam is red, the optical mode is blue, the resonator mirrors are light green, and the undulator is dark green.

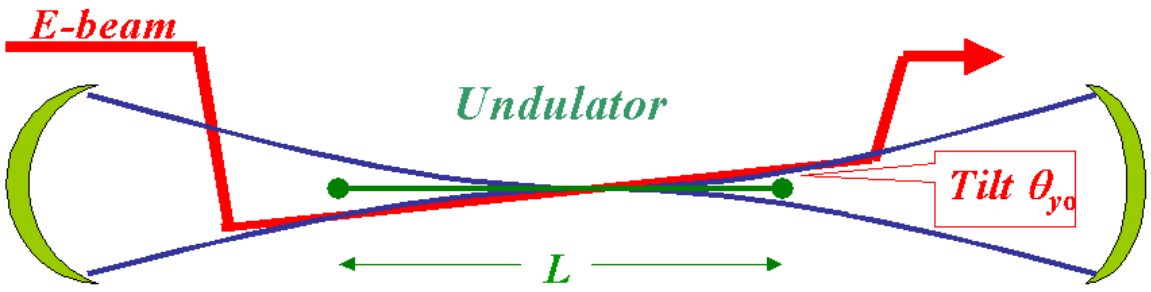

Figure 10 Electron beam tilt. The electron beam is tilted $\tilde{\theta}_{y0}$ about the center of the undulator. The electron beam is red, the optical mode is blue, the mirrors are light green and the undulator is dark green.

a. Electron Beam Tilted at the Center of the Undulator

The results of the study showed a degradation of the extraction with an increase in electron beam tilt. Figure 11 is a plot of the extraction as a function of normalized electron beam tilt. For reference, a tilt of 1 mrad ($\tilde{\theta}_{y0}$=1.4) is shown.

Extraction remains steady for $\tilde{\theta}_{y0} \lesssim 3$ and then starts to decline. Not until $\tilde{\theta}_{y0} \gtrsim 8$ ($\theta_{y0} \approx 5.3$ mrad) does the extraction fall below the level required for 1 MW of power. Since the design tolerance for this system is 20 μrad ($\tilde{\theta}_{y0}$=0.03), the laser would be expected to operate with an extraction of approximately 2.5%, which exceeds the amount required for a MW class laser.

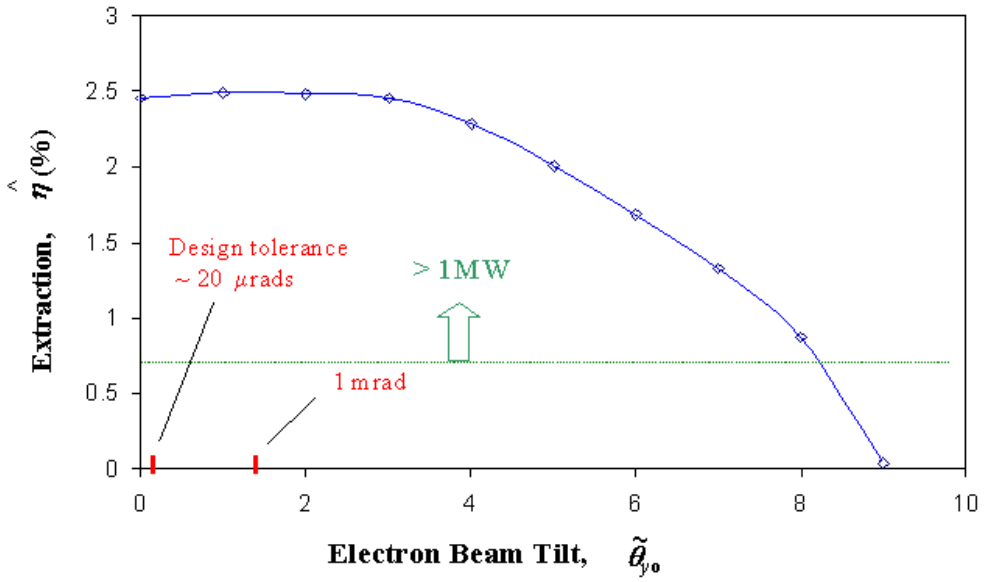

Figure 11 Extraction versus Electron Beam Tilt at the Center of the Undulator. Performance does not degrade until electron beam tilt is greater than $\tilde{\theta}_{y0} \approx 3$, well beyond the design tolerance of 20 μrad.

b. Electron Beam Tilted at the Beginning of the Undulator

Similar to the electron beam tilted at the center of the undulator, simulations show degradation in performance when the electron beam is tilted at the end of the undulator. In this case, however, extraction starts to decrease with even a small tilt and declines with smaller angles than when tilted about the center. Figure 12 is a plot of the extraction as a function of the normalized electron beam tilt. When the electron beam is tilted at the beginning of the undulator, performance starts to decline with small tilt angles, but does not sharply decrease until $\tilde{\theta}_{y0} \gtrsim 1.2$. For $\tilde{\theta}_{y0} \lesssim 1.5$, ($\theta_{y0} \approx 1$ mrad) there

is sufficient extraction for approximately 1 MW of power, which is many times larger than the design tolerance of 20 μrad ($\tilde{\theta}_{y0}$=0.03). Like the previous case, an extraction of 2.5% would be expected even when tilted at the beginning of the undulator. While electron beam tilts lead to small degradations in performance, these simulations show current design criterion is sufficient to maintain laser operation with at least a MW of power.

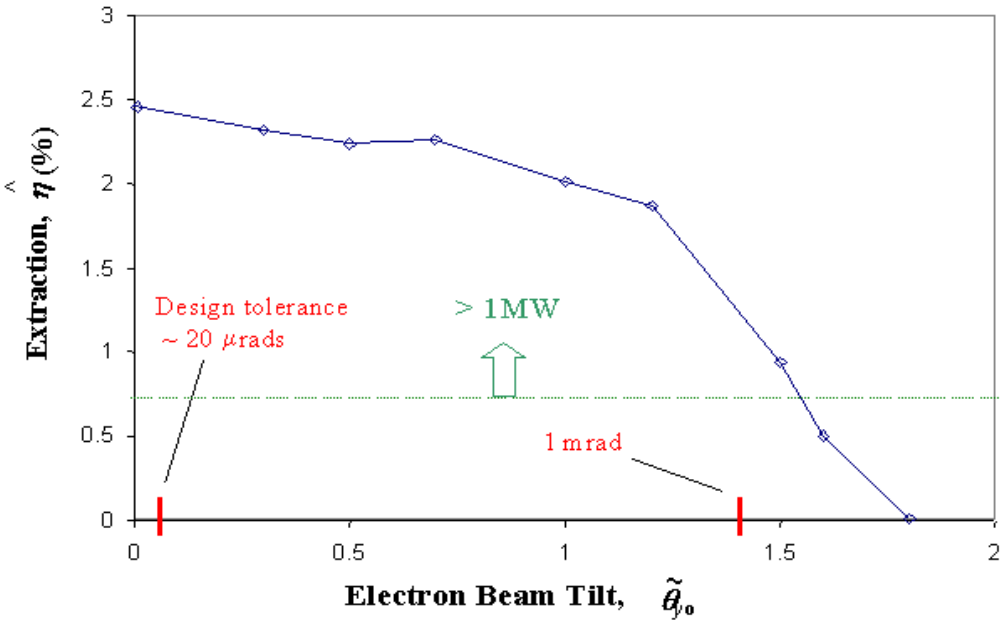

Figure 12 Extraction versus Electron Beam Tilt at the beginning of the Undulator. Performance degrades as electron beam tilt increases and sharply falls off for $\tilde{\theta}_{y0} \approx 1.2$, which is beyond the design tolerance of 20 μrad.

2. Optical Mode tilt

Another source of misalignment studied was a tilt in the resonator mirrors. In a an optical cavity with perfectly aligned mirrors, the optical mode is concentric with the resonator. However, even small perturbations in the position of the mirrors can cause a significant rotation of the optical mode. Figure 13 shows aligned and rotated optical modes in an optical cavity. In this figure, the optical modes are blue and the electron beam is red. The optical mode spot size on the mirror w is shifted a distance δy when

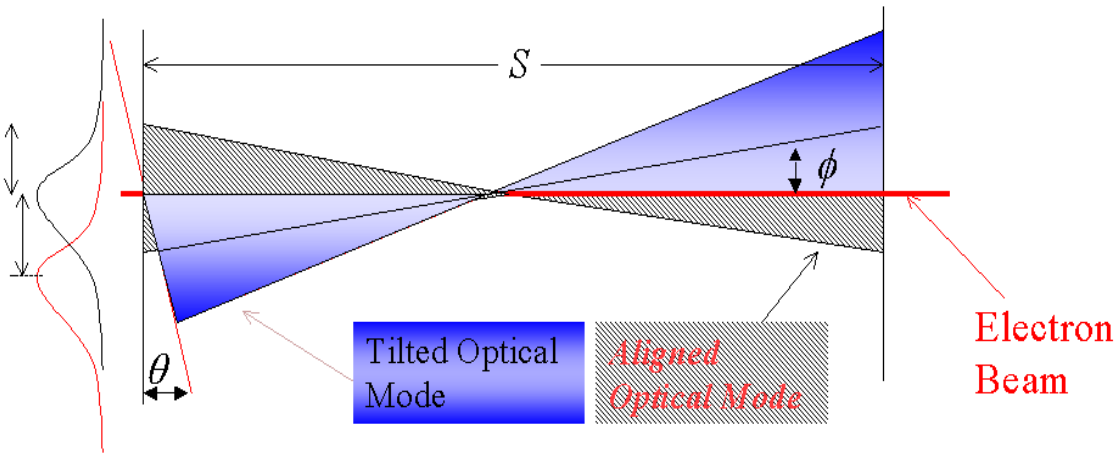

Figure 13 Rotation of Optical Mode due to Mirror Tilt. Mirror tilt angle θ results in a rotation ϕ of the optical mode (shown in blue). As the mode rotates, the electron beam (shown in red) is no longer aligned with the optical mode, which results in degraded performance.

the optical mode is rotated due to a tilt θ in one of the mirrors. Since the greatest intensity of the optical beam is centered along the length of the optical mode, rotations in the mode result in interaction between the electron and optical beams occurring in a region of lower optical intensity. This leads to degraded performance characterized by decreased extraction. Figure 14 shows this rotation and that the electron beam is no longer coincident with the greatest optical intensity. A benefit of the collinear amplification of the FEL is that it realigns the optical mode to the electron beam and the axis of the resonator. This increases the inherent stability of the system.

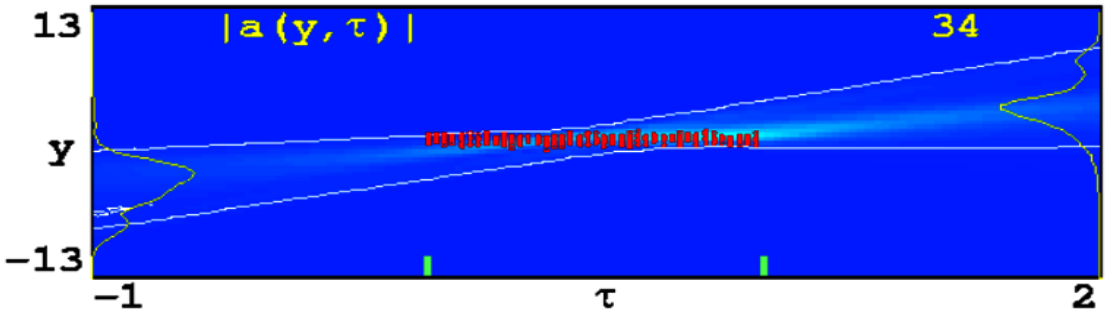

Figure 14 Simulation Output of a Rotated Optical Mode. The optical mode is no longer collinear with the electron beam, so regions of greatest optical intensity due not always contain electrons. This leads to degraded performance. Relative intensities of the optical beam are shown in shades of blue and the electrons are shown in red.

In our study [Crooker] the effect of mirror tilt on the performance of an FEL was investigated. Using the same argument presented for electron beam tilts, one of the

optical cavity mirrors was incrementally tilted and simulations were used to find the maximum steady state extraction. Figure 15 is a plot of extraction as a function of normalized mirror tilt θ_m, where

$$\theta_m = \theta\left(\frac{\lambda}{\pi L}\right)^{-1/2} \tag{4.5}$$

and θ is the actual mirror tilt. For reference, a mirror tilt of 0.1 mrad (θ_m = 0.13) is shown.

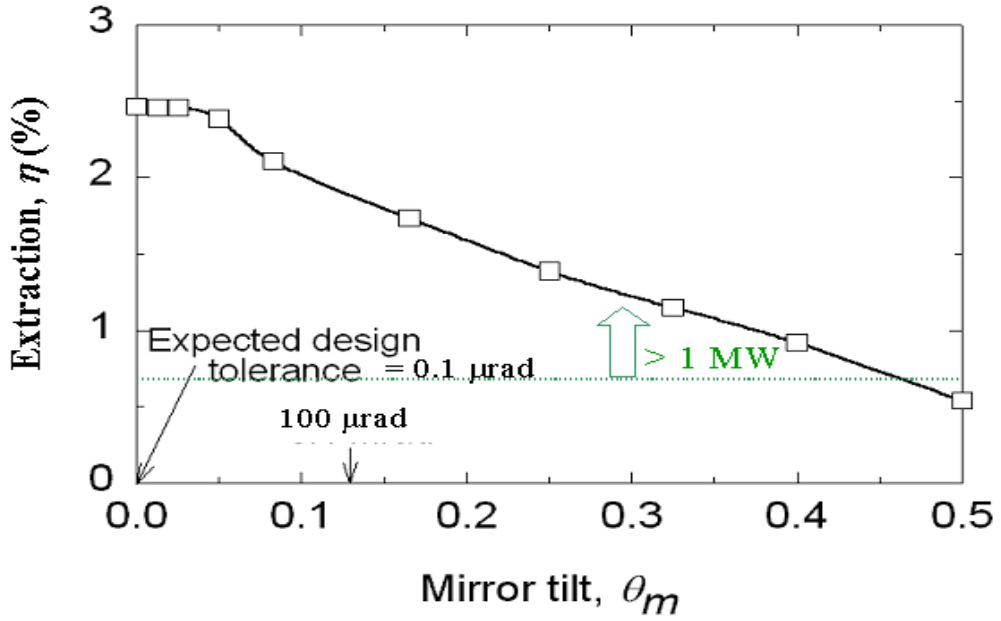

Figure 15 Extraction Versus Mirror Tilt. As the cavity mirror is tilted, performance steadily declines and falls below 1 MW at $\theta_m \approx 0.4$, which is much greater than the design tolerance of 0.1 μrad.

Simulations show, for small tilt angles, there is virtually no degradation in performance. Not until $\theta_m \gtrsim 0.05$ does the extraction begin to steadily decrease and does not fall below the MW threshold until $\theta_m \approx 0.46$ ($\theta \approx 0.35$ mrad). Using active alignment, the system design tolerance is anticipated to be 0.1 μrad, so mirror vibrations would not be expected to significantly degrade the laser performance. For vibrations within tolerance, extraction for this design would remain almost constant ($\eta \approx 2.5$ %), which is more than sufficient for a MW class laser.

The short Rayleigh length design shows promise as a method of preventing mirror damage, but stability becomes a bigger concern. Simulations predict that vibrations degrade performance, but not so much that the laser falls below one megawatt under current design tolerances. Simulation results indicate the design tolerances have some room for relaxation, so the system could be built to accommodate larger variations in electron beam tilt and mirror tilt. Although larger variations would more than likely lead to a larger decrease in performance, a megawatt of power still appears to be possible.

C. OPTIMIZATION OF PARAMETERS

Not only do simulations of an FEL provide an opportunity to explore critical design tolerances, they permit the determination of optimal parameters once a design has been chosen. For example, we studied the parameters for the resonator cavity, undulator, and electron beam for a short Rayleigh length MW-class FEL. Using the same simulation methods as before, the undulator length, Rayleigh length, mirror output coupling, electron beam focusing, and electron beam current were varied in order to investigate each parameter in this design.

The base design used in this study was a short Rayleigh length FEL with N = 14 undulator periods. The undulator period was $\lambda_0 = 2.7\,\text{cm}$, so the length of the undulator was $L = 37\,\text{cm}$. The undulator magnetic field had a peak magnitude of $B = 0.8\,\text{T}$ and the undulator parameter was $K = 1.4$. The electron beam energy was 100 MeV with a peak current of 1500 A and an average current of 1.1 A. The electron bunch length was 0.3 mm long and the electron beam radius was 0.07 mm. The optical resonator was 16 m long and the Rayleigh length $Z_0 = 2.6\,\text{cm}$. This design would generate a 1 μm wavelength, MW class laser beam with a nearly single-mode wavefront and excellent beam quality. When varying each of the design parameters, all others remain fixed at the values mentioned above.

1. Undulator Length

The first parameter studied was the number of undulator. In this study, λ_0 was held constant, and N was vaied from 8 to 20 periods. Figure 16 is a plot of the extraction as a function of the number of undulator periods. For N < 10, the extraction

was zero. For N ≥ 10, the extraction was approximately between two and three percent, and the optimum extraction occurred at about N = 14.

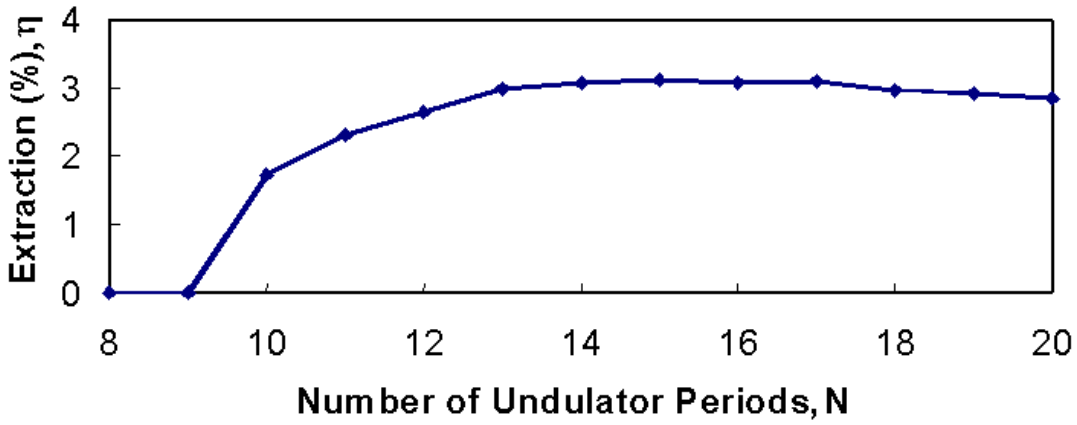

Figure 16 Extraction Versus Number of Undulator Periods. There is no extraction until N ≥ 10. Extraction peaks at N = 14 then slowly degrades.

For N < 10, there were not enough undulator length to sufficiently bunch the electrons and achieve gain above threshold. As the number of undulator periods increased beyond ten, sufficient electron bunching occurred and energy was extracted from the electron beam. The small decrease in extraction for an undulator with more than fifteen periods is due to a lower optical saturation limit. Since the goal is to produce a design as small as possible, an undulator of more than fifteen periods would only add unnecessary size to the device. In a short Rayleigh length FEL, the expanding optical mode can scrape some energy onto the undulator causing damage. Since $\lambda_0 = 2.7$ cm, the optimum undulator length would be approximately 40 cm.

2. Rayleigh Length

The next parameter studied was the Rayleigh length (Z_0) of the optical cavity. Rayleigh length is the characteristic distance over which the spot size of the optical beam grows. From equation (4.3), the Rayleigh length is defined as

$$Z_0 = \frac{\pi w_0^2}{\lambda}. \tag{4.6}$$

In an optical cavity, the Rayleigh length is predetermined by the curvature of the mirrors. Mirrors with high curvature produce a strongly focused the optical beam and result in a

short Rayleigh length. A positive consequence of this focusing is the spot size of the optical beam rapidly expands as it propagates away from the undulator which leads to lower optical intensity on the mirrors, reducing the possibility of mirror damage. However, if the optical beam is focused too tightly, the beam expands too rapidly to optimally interact with the electron beam towards each end of the undulator and may even scrape the outer edges of the undulator. This can cause a decrease in extraction.

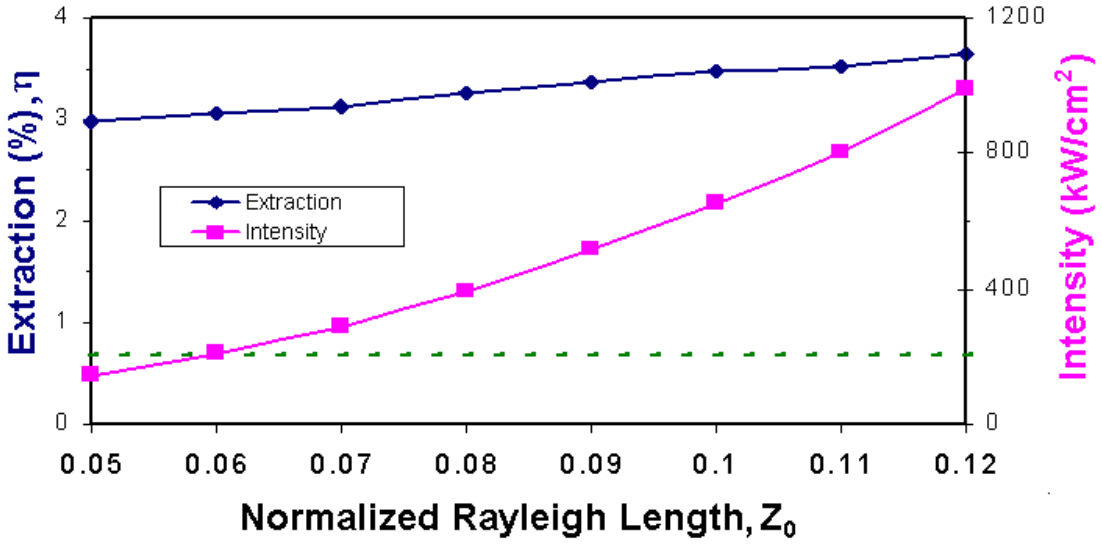

Figure 17 Extraction Versus Normalized Rayleigh Length. Extraction, plotted in blue, slightly increases with Rayleigh length, but mirror intensity, plotted in red, rapidly increases. Intensities greater than ~200 kW/cm^2 (green dashed line) can cause mirror damage. For $\tilde{Z}_0 \lesssim 0.06$, a megawatt class laser would be safe from mirror damage.

Figure 17 is a plot of extraction and mirror intensity as a function of normalized Rayleigh length ($\tilde{Z}_0$), defined by

$$\tilde{Z}_0 = \frac{Z_0}{L}. \tag{4.7}$$

Shorter Rayleigh lengths produce less extraction (shown in blue), but also result in significantly lower mirror intensity (shown in red). Modern cryogenic mirrors can withstand approximately 200 kW/cm^2 of intensity before risking thermal damage. Simulations show an FEL design with resonator mirrors spaced 16 m apart would risk

thermal damage for $\tilde{Z}_0 \gtrsim 0.06$. It is found that a design with $\tilde{Z}_0 < 0.06$ ($Z_0 \approx 2.2$ cm) would have approximately 3% extraction, which is sufficient for a megawatt class laser.

3. Mirror Output Coupling

The third parameter studied was the mirror output coupling. Output coupling is a physical property of the mirror and coating materials, and it describes the fraction of optical energy that passes through the out-coupling mirror of the resonator cavity. The degree of output coupling is described by Q_n, which is the inverse of the output mirror transmittance. For example, $Q_n = 2$ refers to 50 % transmissivity and $Q_n = 4$ refers to 25% transmissivity. For small values of Q_n, a relatively large part of the optical beam is transmitted through the out-coupling mirror, leaving a small amount of power in the optical cavity. Reducing the amount of power in the cavity lowers the intensity on the mirror surfaces, but also lowers the extraction. On the other hand, if Q_n is large, more of the optical power is contained in the cavity. This leads to an increase in extraction, but also an increase in mirror intensity.

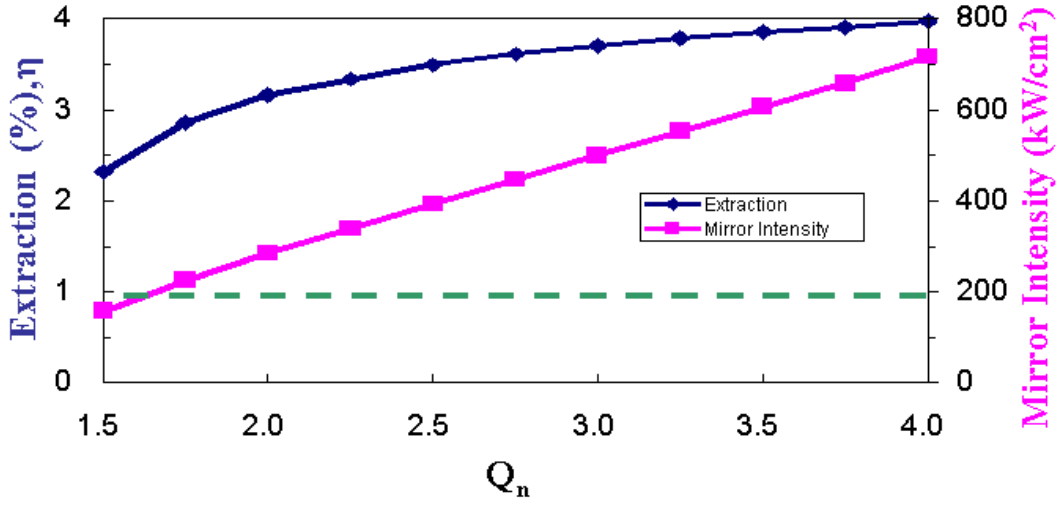

Figure 18 Extraction Versus Output Coupling. As Q_n increases, the extraction (blue) steadily increases, but so does the mirror intensity (red). Intensities $\gtrsim 200$ kW/cm^2 (green dashed line) can cause mirror damage, $Q_n \lesssim 1.7$ should be selected for this design. Doing so results in approximately 2.5 % extraction, which is sufficient for a MW class laser.

Figure 18 shows the extraction (blue) and mirror intensity (red) as functions of Q_n. As Q_n increases, the extraction steadily increases, but so does the intensity on the mirrors. Mirror damage is likely to occur for intensities greater than 200 kW/cm^2, which is shown by the green dashed line. In order to prevent mirror damage, a design with $Q_n \approx 1.7$ (~60 % transmission) should be chosen. In this case, the extraction would be approximately $\eta \approx 2.5$ %, which is sufficient for a MW class laser.

4. Electron Beam Focusing

The fourth parameter studied was the electron beam focusing. For this parameter, both the position and electron beam radius at the focus were investigated. In the short Rayleigh length design, the optical beam is intensely focused at the center of the undulator, resulting in a rapid change in optical beam amplitude and phase near the midpoint. Since the greatest intensity of the optical beam is at the center of the undulator, the electron beam should also be focused at the center in order to optimize the overlap with the optical field.

The emittance of the electron beam is a fixed product of the electron beam radius (r_b) and divergence (θ_b), so a small radius results in a rapidly diverging beam, while an electron beam with a large radius does not diverge as rapidly. Figure 19 shows the relationship between the radius and divergence of the electron beam. It is important to optimize the electron beam radius in order to achieve the maximum interaction between the optical field and the electron beam. If r_b is too small, the electron beam rapidly

Figure 19 Electron Beam Emittance. Since emittance is a fixed product of r_b and θ_b, an electron beam with a small radius has a large divergence while an electron beam with a large radius has a small divergence.

diverges and does not fully interact with the optical beam at the ends of the undulator, which decreases the extraction. On the other hand, if r_b is too large, the electron beam will not diverge as rapidly, but the interaction between the beams will decrease at the center of the undulator, which also decreases the extraction.

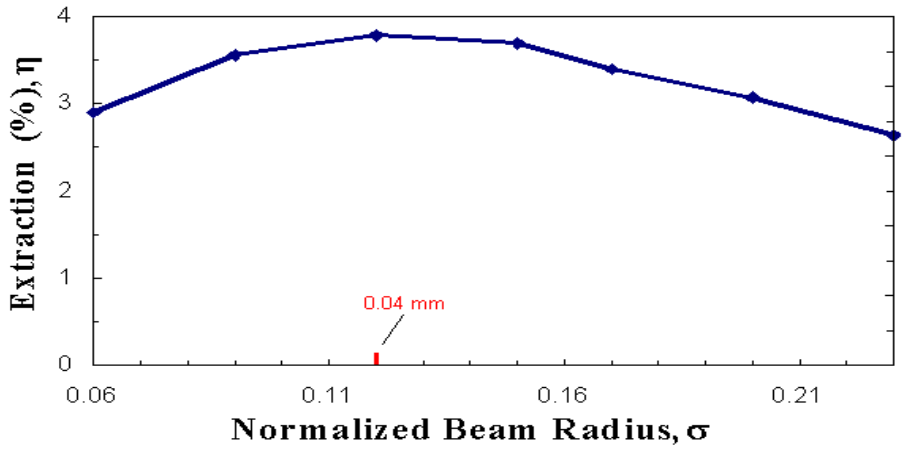

Figure 20 Extraction Versus Normalized Electron Beam Radius. Optimum extraction occurs when $\sigma \approx 0.12$ ($r_b \approx 0.04$ mm). A smaller radius diverges outside of the optical mode at the ends of the undulator and larger radius is outside of the optical mode at the center of the undulator.

Figure 20 is a plot of the extraction as a function of the normalized electron beam radius (σ), given by

$$\sigma = r_b \left(\frac{\pi}{L\lambda} \right)^{1/2}. \tag{4.8}$$

Maximum extraction would be expected when $\sigma \approx 0.12$ ($r_b \approx 0.04$ mm) shown in figure 20. A smaller electron beam radius diverges outside of the optical mode towards the ends of the undulator, but a larger electron beam does not fully interact with the optical mode at the center of the undulator. Figure 21 is a simulation output of a tightly focused electron beam, where, $\sigma = 0.06$, ($r_b = 0.02$ mm). The electron beam (red) has an hour glass shape and is contained by the optical field (blue) at the center of the undulator. However, as the electron beam diverges, it interacts with fields of lower intensity at each of the ends of the undulator, resulting in less than optimum extraction.

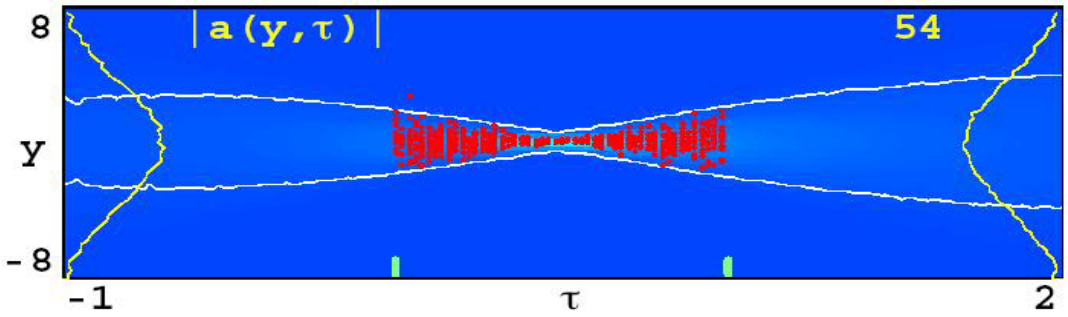

Figure 21 Example of a Focused Electron Beam. The small electron beam radius (r_b = 0.02 mm) is contained by the optical mode at the center of the undulator, but diverges outside of the optical mode at the each end of the undulator.

5. Electron Bunch Charge

The final parameter studied was the electron beam current by varying the micropulse bunch charge (q) at 750 MHz repetition rate. As the bunch charge is increased, the electron beam current increases, but so does the emittance. Increasing the emittance increases the design tradeoffs between the electron beam radius and divergence discussed in the previous section. Therefore, it would be ideal to determine the minimum current required to meet the design goals of the system.

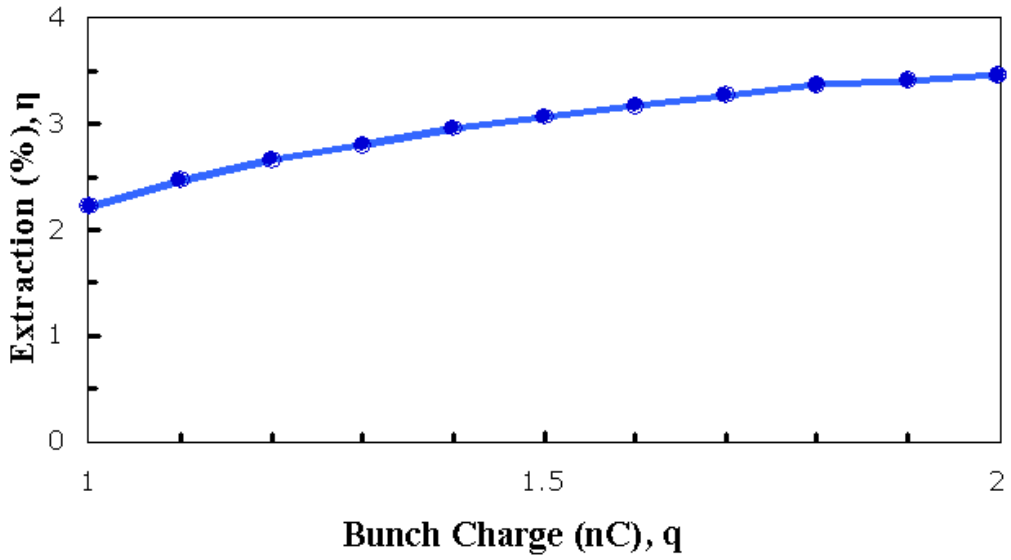

Figure 22 Extraction Versus Bunch Charge. Extraction increases with bunch charge, but so does extraction. A bunch charge of 1 nc is sufficient to achieve a MW class laser and simultaneously minimizes the emittance.

Figure 22 is a plot of the extraction as a function of bunch charge. As the bunch charge increases, so does the extraction. For this simulation, the emittance was assumed to remain constant, but would most likely increase with the bunch charge. Since larger emittance tends to lead towards a decrease in extraction, a system with $q \approx 1\,\text{nC}$ would be expected to perform a little better than the plot suggests while a system with $q \approx 2$ nC would not quite do as well as predicted. The simulations suggest $q = 1\,\text{nC}$ would provide sufficient current for a MW class laser.

In this study, the effects of the undulator length, Rayleigh length, output coupling, electron beam radius and electron beam current on extraction were investigated. The optimum undulator length was found to be L = 40 cm long. The optimum Rayleigh length was found to be Z_0 = 2.2 cm long. The optimum Q_n was found to be 1.7, or approximately 60% transmission. The optimum electron beam focal point was at the midpoint of the undulator with a radius of r_b = 0.04 mm. Finally, the optimum electron beam bunch charge was found to be q = 1 nC. In each case, the requirements for a MW class laser were met, demonstrating the short Rayleigh length design is a viable option for a free electron laser weapon system.

V. CONCEPT OF OPERATIONS

In order for a free electron laser to be considered a viable weapon system, the operational employment of the system must be explored. This employment includes, but is not limited to, operational use, shipboard integration and mission capabilities. Since space on a ship must be fully optimized, weapon systems must be capable of fulfilling multiple missions. Additionally, it should be able to incorporate pre-existing systems. The operation and integration of the FEL will be discussed with specific reference to the detect-to-engage sequence, followed by scenarios of FEL employment in various mission areas.

A. DETECT-TO-ENGAGE SEQUENCE

One of the principle areas of consideration for a tactical watch stander is the detect-to-engage sequence. This sequence of events covers each step of an engagement from the first time a target is discovered until it is no longer a threat. For each hostile target, the sequence starts with detection and terminates with battle damage assessment.

1. Detection

The first step in the detect-to-engage sequence is detection. Onboard a ship, there are multiple sensors at any time searching for contacts. Some, such as radar, are active systems that radiate and analyze reflected energy. Others, such as infrared or visual cameras, are passive, which depend on the ability to detect the contact's own emissions. It would be unlikely to use an FEL for target detection, so it must be integrated with existing sensor systems. Because no system is perfect, not all detected signals turn out to be contacts, which leads to the next step in the sequence.

2. Evaluation

Once a signal has been detected, the next step is to evaluate the likelihood it indicates a real contact. This is typically done with a signal processing algorithm tailored to the detecting sensor. Some targets turn out to be random noise or animals (birds, whales, etc.), but others are true contacts and will be tracked.

3. Track

The next step in the sequence is to establish a track on the target. In this context, track refers to determining the contact's position and predicting its next position, and should not be confused with any particular weapon system acquiring and "locking" a target. An FEL would likely be capable of tracking a target within visual range, but most likely it would not be used this way for various reasons. First, tracking with a weapon system is considered an act of hostile intent and could escalate an otherwise benign situation. Second, tracking an unidentified target engages the beam director. In the event another target must be engaged quickly, some time would be lost while dropping the track and acquiring the higher priority target. Besides, other shipboard systems, such as track while scan radars, are better suited for tracking and providing information about unidentified contacts.

4. Identification

Once a track on a contact has been established, the next step is to identify (ID) the target. From the track history, the range, course, speed, and altitude (for air contacts) can be determined. If the contact has a detected emission, then information can be obtained using shipboard libraries. For air and some surface contacts, Identification-Friend or Foe (IFF) interrogations often provide specific information about the platform. If the contact is in visual range, then recognition programs or even an operator at a console can provide a positive ID. Among the ways an FEL could assist in target identification is through visual recognition, where the optical systems could be trained on a radar contact's line of bearing and an operator could see the source. Another way an FEL might ID a target is by blade-counting. It is feasible that an FEL, operating at a very low power, might be able to determine the number and rotation rate of turbine blades on an aircraft. Similar to sonar systems counting propellers, this information, coupled with an onboard library, could potentially determine the type of aircraft or even the exact plane.

5. Threat Assessment

Once a contact has been identified, the relative threat it presents to the ship can be evaluated. Some contacts, such as a supersonic inbound missile, present an immediate threat and will need a partially, if not fully, automatic engagement. Others, such as a

fishing vessel, might not even be a threat and definitely require a decision by an experienced watchstander. For most cases, this is a step performed by an operator sitting at a console in the Combat Information Center (CIC). However, ships are capable of utilizing pre-programmed procedures, known as doctrine, to recognize and engage high threat contacts when there is not enough time for someone to make a conscious decision.

Since threat assessment is a function performed by an operator or the combat system suite, an FEL weapons system would not directly be used for this step. However, an FEL operator might be using the beam director to observe a contact and would need the ability to rapidly respond to a change in the threat assessment, such as a fisherman suddenly aiming a shoulder-fired missile at the ship. In addition, control of the FEL weapon system must be able to automatically shift to a higher priority threat, even if it means overriding the operator in accordance with the programmed doctrine.

6. Weapons Pairing

Ships use a combination of pre-programmed fire control procedures and established combat systems doctrines to determine the appropriate weapon to respond to an established threat. Since the primary advantage of an FEL is a speed of light engagement, it must be capable of automatically engaging a high threat target, even if that requires taking control from an operator. In most cases, the FEL will not be tracking the target until assignment. Track information, such as bearing, range, and predicted position will have to be automatically passed to the FEL. For a high speed inbound target, the FEL may only have seconds to slew to the threat bearing, acquire the target and fire. Simultaneous initiation of the cathode drive laser, electron injection and accelerator RF fields will be required so the laser is ready to fire when ordered.

Besides a speed of light engagement, another reason the FEL would be the chosen weapon for an engagement is its surgical accuracy. Since the system most likely will use a low power beacon laser for adaptive optic atmospheric corrections, this same beacon permits the operator to see exactly where the weapon is pointed. Missiles and bullets get close, but certainly no more accurate than a couple of meters, often farther away. All an FEL operator has to do is verify that the beacon is where the high powered beam should go, and then “pull the trigger”.

7. Engagement

After the proper weapon has been selected, the target has to be engaged. For an automatic engagement, the fire command would be sent to the FEL from the combat system suite at a predetermined maximum engagement range. Time (a few seconds) often elapses after a weapon system has been paired to a target and before the engagement occurs in order to optimize the tactical situation. For a manual engagement, the FEL operator would be ordered to engage a specific track, which he would assign to the weapon system. The FEL would then be "slaved" to follow that track until the operator engages the contact, drops the track, or the system is automatically reassigned to another, higher priority track.

8. Battle Damage Assessment

The final step in the detect-to-engage sequence is battle damage assessment. This is an evaluation of the effectiveness of the engagement. A successful engagement can be verified by observing the destruction of the target visually, hearing underwater explosions with sonar, or watching the altitude of a radar contact drop to sea level before losing the track altogether. On the other hand, observing the radar return of a self-defense missile pass by the target without detonating, or visually watching the target survive an explosion are indicators of an unsuccessful engagement. Battle damage assessment is crucial so the watchstander knows if the target is still a threat or if he can direct his attention elsewhere.

There are a number of ways an FEL would actively contribute to battle damage assessment. The likeliest way would be to have the FEL operator sitting at the console watching the engagement and seeing the target's destruction. Another way might be the beam director control system detecting the target's sudden transition to erratic flight. The sudden loss of the return from a beacon laser might indicate a loss of target. One independent method of performing battle damage assessment is observations from another platform, such as a manned aircraft, an unmanned aerial vehicle, or even satellite imagery. Another method is the loss of the contact from shipboard radar or sonar. In order for the watchstander to maintain the accurate tactical picture, information from the FEL as well as other systems must be simultaneously processed. Shipboard integration is crucial for a successful FEL engagement.

B. INTEGRATION

When weapon systems were first installed on ships, the entire system primarily functioned as a sovereign unit. Search radars would detect the contact, and then it would be identified and declared hostile. Finally, an independent fire control radar would find and illuminate the target for the gun or missile system's engagement. Modern naval vessels do not have the space or the manpower to support independent systems, so most are multi-purpose and are fully integrated. For example, the Naval Tactical Data System (NTDS) receives contact data from air and surface radars, electronic emission sensors, and sonar to create one composite picture for the watchstander. If necessary, designated contact data can then be "handed off" to a weapons system for engagement. The AEGIS combat system is even more integrated and can be programmed to automatically track, and if necessary, engage a hostile target. The next generation volume search radar will be even more automated and the FEL weapon system will need to be capable of full integration for maximum effectiveness.

1. Command and Control

Integration does not only involve equipment interaction, but relationships between watchstanders as well. Onboard a ship, the Commanding Officer (CO) has absolute authority and ultimate responsibility for everything. The CO has the prerogative to delegate authority to watchstanders, but can never give up his responsibility for the ship. This means a subordinate watchstander can authorize an engagement, but the CO will be held responsible for the results. For this reason, only personnel that have earned the CO's trust will stand a watch with the authority to initiate an engagement.

The primary watchstander with this responsibility is the Tactical Action Officer (TAO). This watchstander answers directly to the CO for all combat operations and is responsible for managing the Combat Information Center (CIC). In CIC, various watchstanders operate system consoles in order to detect, track, identify, and, if necessary, engage contacts.

Two principle watchstanders working directly for the TAO are the Track Supervisor and the Ship's Weapon Coordinator (SWC). On some ships, the SWC

watchstation is called the Weapons Coordinator Console (WCC), but SWC will be used to denote this watchstation. The Track Supervisor manages all contact information by correlating data from various search radars, sonar, and electronic emissions. The SWC supervises all weapon system watchstanders. In a high threat scenario, the Track Supervisor would alert the TAO of a hostile contact, then the TAO would make the decision to engage and give the batteries release order to the SWC. The TAO may designate which weapon system to use or he may leave it to the discretion of the SWC to engage the target in accordance with the CO's Battle Orders. In either case, the SWC then passes the batteries release order to the specific weapons system console operator for the engagement.

The above steps assume a fully manual engagement. Weapons systems can also be configured in semi-automatic or automatic mode. In a semi-automatic configuration, the NTDS will automatically perform some of the steps of the engagement, such as handing the track off to the weapon system. Under some circumstances, the SWC might push the firing button as well. Semi-automatic control is normally used for time sensitive engagements, such as supersonic anti-ship cruise missile defense, where the speed of automation is required, but a watchstander still has to manually initiate engagement. When in automatic mode, all the watchstanders can leave CIC and the ship will engage targets according to its doctrine. This mode is rarely used because of the hazards associated with losing control of a weapons system, but might be needed in extreme circumstances.

2. Fire Control

Fire-control integration involves the mechanical and electronic interaction between the various sensor and weapons systems on the ship through the detect-to-engage sequence. Ships typically employ independent air and surface search radars as well as sonar to actively search for contacts. Simultaneously, electronic emissions from contacts are monitored and correlated to build the tactical picture. In addition, off-ship information, such as contact reports from other ships, is added to increase situational awareness. These different systems would not function if they were not integrated into the ship's combat system. For example, consider a high speed inbound target detected by

the air search radar. The radar can determine the bearing, range, and velocity of the target, and data processing algorithms can predict where the track is going. Once the TAO determines the contact is a threat and orders batteries released for the FEL, the known bearing, range, velocity and predicted position must be passed on to the fire control system for engagement and the beam director must train to the appropriate bearing and azimuth. The systems would have little value if they could not share information.

3. Tactical

In complex battle scenarios, it is possible for multiple inbound targets to saturate any given weapon system. Integration provides the ship a divide and conquer capability, where the multiple targets can be assigned to different weapon systems for simultaneous engagements. For example, a common threat in littoral warfare is the swarm raid. In a swarm raid, as many as 50 small speed boats or jet skis simultaneously approach the ship in a coordinated attack. In order for a warship to defend itself against this tactic, it would need to be able to engage with missiles, guns, and small arms in an integrated counter attack. Each weapon system would be assigned an individual target based on priority. As each target is destroyed, the successful weapon system would need to be paired with another target. Only a fully integrated combat system suite would be able to successfully counter a swarm raid.

Another specific example of how an integrated defense is advantageous is against a high speed, high G terminal maneuver cruise missile. This type of cruise missile rapidly approaches the ship. A few seconds before impact, it starts to radically alter course in such a way that defensive missile and gun systems can't keep up. Integrating an FEL into the defensive weapon system eliminates this advantage. An inbound missile that performs multiple turns cannot outmaneuver the laser and will expose its wings and body to the beam. The same flight profile that is disadvantageous for missile and gun systems is preferable for the FEL. In contrast, an inbound missile that does not maneuver only exposes its nose cone to the FEL. Since the cruise missile's wings and body are easier to destroy with a laser beam than the nose cone, the head on shot is more challenging for an FEL. However, this same flight profile is easier for missile and gun

systems to engage since the target is not maneuvering. If missiles, guns, and an FEL are simultaneously employed against an inbound cruise missile, then the type of terminal maneuver it employs will give at least one of the systems an advantage against it.

C. SCENERIOS

Operational scenarios will be presented in order to continue to explore how an FEL can be integrated into the ship's combat system. One of the primary advantages of the FEL is a speed of light engagement, which would be utilized against a supersonic anti-ship cruise missile attack. Another advantage of the FEL is its surgical precision that will be used in a scenario against a hostile boat surrounded by neutral surface contacts. Both the surgical precision and speed of engagement makes the FEL a potential candidate for surface fire support of an amphibious landing by using a relay mirror mounted on an Unmanned Aerial Vehicle (UAV). Although technologically challenging, the basics of the scenario will be explored in order to determine how feasible such a use might be.

1. Anti-ship Cruise Missile Attack

In this scenario, consider a Nimitz class aircraft carrier operating in open waters. An advanced version of the SS-N-22 SUNBURN anti-ship cruise missile (ASCM) is launched against the carrier from a range of 30 km. Since the current SS-N-22 has a maximum speed of Mach 2.2 at 20 m above the sea surface, this scenario will assume the advanced version has a maximum speed of Mach 3 at 10 m above the surface. Figure 23 illustrates how the curvature of the earth limits the detection range of the missile.

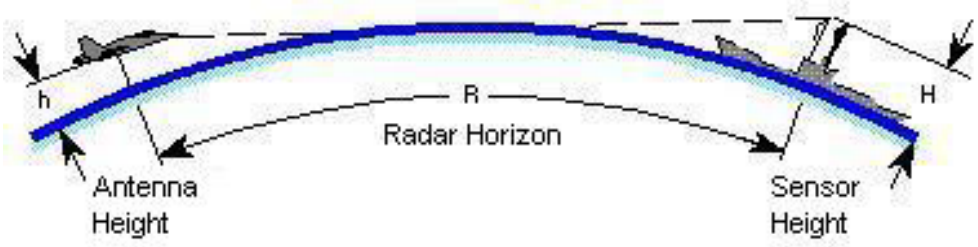

Figure 23 Radar Horizon Range. After [EW & Radar Handbook] The curvature of the earth limits the maximum detection range of a contact. This range (R) depends on the height of the sensor (H) and the altitude of the contact (h).

The maximum detection range is called the "radar horizon range" and is calculated using equation (5.1), where R is the radar horizon range in kilometers, H is the height of the sensor in meters, and h is the altitude of the contact in meters.

$$R = 4.12(\sqrt{H} + \sqrt{h}) \tag{5.1}$$

Considering the height of a radar antenna on the carrier is approximately 20 m and the altitude of the ASCM is 10 m, the maximum detection range based on the radar horizon is 31.5 km. Because radar systems are affected by external factors, such as sea clutter, atmospheric conditions, or even other sensors, they rarely detect a contact at the radar horizon. The maximum effective range is normally between 80 and 90 percent of the radar horizon range. In this case, the missile would first be detected at approximately 26 km. The speed of sound is 343 m/s at sea level, so at Mach 3, the velocity of the ASCM is approximately 1000 m/s. A simple time-distance calculation predicts the missile will impact the carrier in 26 seconds.

The carrier cannot detect the cruise missile until it closes within the radar horizon. The first detection could occur at 31.5 km, but would more likely occur at 26 km by the Target Acquisition System (TAS) radar, which is a radar specifically designed to search for high speed, low altitude contacts. Since the TAS antenna rotates at 30 RPMs and the system requires 3 hits to recognize an inbound threat, the cruise missile would be about 22 km away when CIC is first alerted to its presence. At Mach 3, the missile is now 22 seconds away from impact.

Not only is TAS integrated with NTDS, but it can directly share information with the Nato Seasparrow Missile System (NSSMS), which uses an eight canister box launcher to fire the RIM-7 Seasparrow missile. In the event of an inbound, high speed contact, TAS will automatically pass targeting data to the NSSMS. The missile director will automatically train and illuminate the threat while the missile launcher trains and elevates in preparation of firing. The FEL Weapon System (FELWS) would most likely be similarly integrated so that the beam director automatically trains, elevates, and locks on the target. The low power beacon laser would illuminate the target in order for the adaptive optics to start sampling and correcting for the atmosphere.

In CIC, all watchstanders are immediately alerted to the presence of a high speed threat by an audible alarm and onscreen symbology. Figure 24 shows examples of an NTDS screen and some common track symbols. Circles represent friendly contacts,

squares represent unknown contacts, and diamonds represent hostile contacts. Full shapes are used to represent surface contacts, upper halves of the shapes are used to represent air contacts, and lower halves of the shapes are used to represent undersea contacts (not shown). The NTDS screen on the left places the ship in the center of the screen and uses a plus sign as its symbol. The lines originating from each symbol are called speed leaders and represent each contact's velocity. The longer the speed leader, the faster the contact is going. Assuming it takes approximately 6 seconds for the TAO to recognize the threat and order an engagement, the range to the missile is now 16 km and time to impact is 16 s.

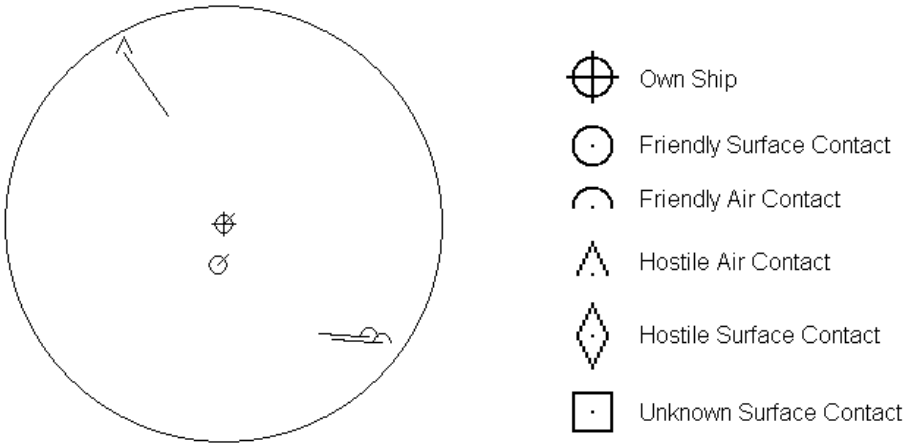

Figure 24 NTDS Symbology. The left hand figure is an example of how an inbound cruise missile would be represented on a tactical console. The icons depicted on the right are some of the more common NTDS symbols.

At 16 km, the inbound cruise missile is inside of the maximum range of the NSSMS, so missiles will immediately launch after the fire button is pushed in a semi-automatic configuration or automatically launch in an automatic configuration. Assuming it takes about one second for missiles to launch, the range of ASCM is 15 km. Current tactics use what is known as shoot-shoot-look-shoot, which means two missiles are simultaneously fired at the target and their performance is evaluated before firing another salvo. Therefore, two RIM-7 missiles would be fired against the SS-N-22. Considering the velocity of the RIM-7 is Mach 2, time-distance equations can be used to determine the cruise missile will be intercepted by the first salvo in 9 seconds at a range of 6 km.

Assuming the maximum effective range of the FELWS is 10 km, the laser would most likely be programmed to track the target and open fire when it crosses that range if the firing button has been pushed or if in an automatic mode. At 10 km, the outbound RIM-7 missiles have been in the air for 5 seconds and are 6.7 km away from the SS-N-22. Once the target crosses 10 km, the FELWS fires a MW laser beam that immediately reaches the target and starts heating the nose cone. Approximately 5 MJ of energy is required to damage the missile, so an engagement with a 1.5 MW FEL would be over in about 3 seconds. At Mach 3, any change in the surface of the nose (such as a 5 cm hole) would cause it to immediately lose aeronautical stability and lose control. From this point on, the missile will fly erratically, break up due to increased drag or structural instability, or dive into the ocean.

The SS-N-22 considered above would be about 7 km away from the ship when it was neutralized. The RIM-7 missiles are 8 seconds into flight and are about 0.5 km away. If the target remains intact, they will continue to close the target and detonate close proximity fuses. If the target breaks up or plunges into the water, the RIM-7's will continue to fly until exhausting their fuel. In this scenario, the FEL destroyed the target about a second before the RIM-7s, but the engagement was based on a near-perfect case situation. Had the ASCM been detected later due to less than optimum radar conditions, the engagement order would have come later and the NSSMS timeline would have followed. On the other hand, the FELWS had to wait 5 seconds before opening fire and a delayed detection would not have impacted its timeline.

2. Small Boat Attack

In this scenario, an FEL equipped DD(X) is conducting Maritime Interdiction Operations in the Arabian Gulf. It has stopped an unidentified merchant ship for boarding and has taken station 1000 m astern. As the boarding team approaches the merchant ship, a high-speed surface contact is detected by surface radar, 4000 m off the starboard beam. CIC quickly determines the unknown contact is on an intercept course with the boarding team and will reach them in about 3 minutes. To make matters worse, there are two surface contacts previously identified as fishing vessels in close proximity to the contact. Figure 25 uses standard symbology to show the surface picture.

Using a video camera, CIC is able to visually identify the contact as a speedboat with five men holding small arms. The ship hails the speedboat and directs them to alter course and stay clear of the area. The speedboat does not answer any of the ship's calls, but continues to close on the boarding team. The TAO determines the speedboat is a hostile threat and orders the FEL operator to manually lock on the target. Using the video camera, the men in the speedboat are observed chambering rounds. The TAO considers this hostile intent and orders the FEL operator to engage the speedboat. The current range is 3000 m, which is within the effective range of the FEL, so the laser immediately fires.

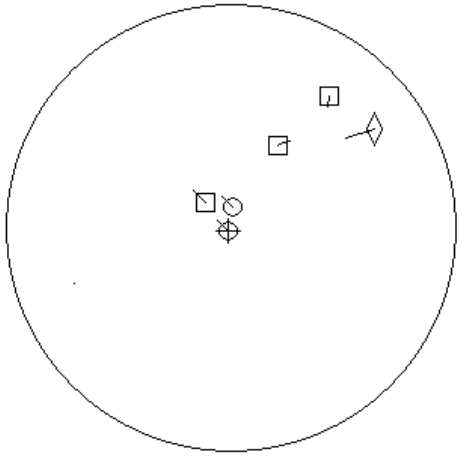

Figure 25 Scenario Surface Picture. The DD(X) is represented by the circle with a plus in the center of the screen. The other circle represents the boat the boarding party is using to approach the merchant ship, which is represented by the square near the center of the screen. The two neutral fishing vessels are represented by two squares in the upper right and the hostile speedboat is represented by a diamond.

When the laser beam hits the speedboat, it will likely burn through a control wire, fuel line, or spark plug cable, which would almost immediately disable the engine. Even if the laser beam does not hit a vital component, it can still be used to overheat the engine. Assuming the speedboat has a 200 HP engine and using

$$1 \text{ HP} = 0.7457 \text{ kW}, \tag{5.2}$$

the power is approximately 150 kW. If the engine operates at 20% efficiency, then the maximum power the engine can sustain is about 750 kW. Even if a 1 MW FEL lost 10% of the power in the optical beam due to atmospheric scattering and absorption, 900 kW of

power would be delivered to the speedboat, which is sufficient to overheat the engine after a few seconds of lasing. Using the video camera, smoke can be seen coming from the outboard engine and CIC observes the speedboat stopping. After a few more seconds of observation, CIC confirms the speedboat has stopped and is drifting, which indicates the engine has been disabled. Since the speedboat is no longer a threat, the attention of the ship returns to its primary duty of boarding the merchant ship for inspection.

The precision of the laser permits the ship to disable the speedboat without fear of collaterally damaging other contacts. It is even likely that the occupants of the speedboat would be unharmed, assuming minimal side lobe affects. This gives the ship the option to engage a target after hostile intent is observed, but before being shot at. Having the ability to engage a target before being shot at gives the defender a significant advantage.

3. Naval Surface Fire Support

In this scenario, an FEL utilizes a reflective mirror on a UAV in order to "bounce" the beam over the horizon, assuming that the enormous technical challenges associated with it are solvable. A Predator UAV will be used with a gyroscopically stabilized mirror as its payload. Figure 26 shows how a UAV can be used to extend the operational range of the FEL over the horizon. Because of size and weight, it is unlikely an adaptive optic system would be incorporated on the UAV. What is more reasonable is a beacon laser from the ship reflects off the aerial mirror and hits the intended target. Reflected radiation returns to the aerial mirror and back to the ship. The round trip samples the atmosphere the high power beam will travel through and provides the information required by the adaptive optic system.

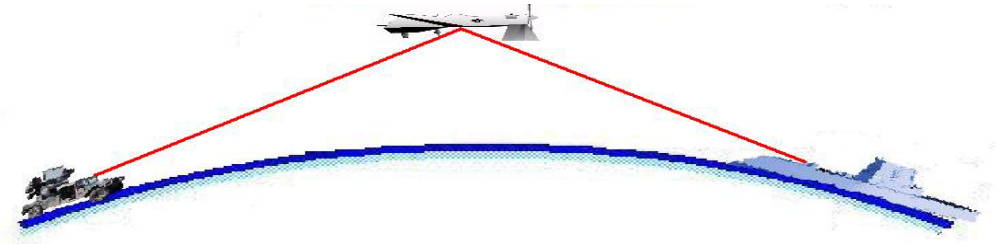

Figure 26 Over the Horizon Engagement. An FEL equipped ship bounces the laser beam off an orbiting UAV in order to engage a target beyond the horizon.

This scenerio assumes a Wasp class LHD that is supporting an amphibious landing of US Marines. For Naval Surface Fire Support (NSFS), the ship has an FELWS.

NSFS permits a light force to call in for heavy fire against a known enemy position without having to actually carry the weapons or ammunition during the landing. It is similar to calling for an air strike, but the ship can remain on station in support of the troops for a longer period of time. As the Marines make landfall, they start receiving hostile fire from six enemy vehicles about 500 meters inland. One of the Marines has a laser designator and uses it to illuminate one of the trucks generating hostile fire. Energy from the laser designator scatters in all directions, so a fraction of it reflects off the target, travels through the atmosphere, and is detected by a sensor on the UAV positioned approximately halfway between the ship and the shoreline. The UAV uses the laser designator to determine the bearing and declination of the target and the known bearing and declination of the ship to appropriately position the reflector.

Less than a second after the target is designated, the UAV reflector is aligned and the beacon laser from the ship is aimed toward the UAV. Light from the beacon laser bounces off the reflector on the UAV and reaches the target. Scattered light then returns to the ship via the UAV reflector. It would be advantageous if sensors in the UAV were designed to compare the bearing and declination of the reflected beacon laser with the reflected laser designator beam. If they are the same, then they are traveling the same path and the FEL is "locked" on the target. If they are different, then the two beams are coming from two different points and the FEL needs to be slightly adjusted. This type of comparison could also be adapted into a control loop to keep the FEL and reflector properly aimed throughout the engagement.

Less than two seconds after designation, the FEL is "locked" on the target. After the TAO confirms the laser is properly targeted, batteries release is ordered and the laser is fired. It would be unlikely for this type of engagement to be in any mode other than manual. That way, an operator can use his console to visually verify the FEL is targeted on the UAV reflector. When fired, the high power laser beam leaves the ship, bounces off the UAV, and strikes the designated truck. Assuming it takes the CIC watch team less than three seconds to verify and fire the laser, it would have taken less than five seconds from the time the target was designated for light to reach the target. Assuming a

three second engagement time and two seconds for the Marine to designate the next target, the FEL could neutralize all six of the hostile trucks in less than one minute.

One of the inherent problems with using a UAV as a reflecting platform is beam alignment. If the high power beam starts to "walk off" the center of the mirror, it could damage the UAV. One way to prevent this is to add intensity sensors along the perimeter of the mirror. If the center of the spot made by the beam drifts towards the edge of the mirror, the intensity will increase. A signal could then be transmitted back to the ship to steer the beam away from that side of the mirror. This signal should be incorporated into the control algorithm already employed by the beam director.

THIS PAGE INTENTIONALLY LEFT BLANK

VI. CONCLUSION

In movies about the Wild West, the bad guy wore black and always drew his gun first. Only then did the hero (played by John Wayne) draw his own weapon and shoot the gun out of his enemy's hand. This is the role the United States military has to play as the world's superpower. A free electron laser brings the U.S. Navy one step closer to this ideal. Because of its speed and accuracy, a hostile force can act first, but an FEL equipped ship can react faster and successfully engage defend against the enemy's engagement.

Modern advances in FEL development makes developing a high energy laser for naval platforms a possibility, and the short Rayleigh length design appears to be a viable option. Simulations predict the stability of a compact, short Rayleigh length FEL can be easily maintained using design tolerances that are achievable with current technology, permitting an optical beam power of at least one MW. An electron beam can be tilted on the order of a milliradian and still generate aporoximately one MW of power. This is well below the design tolerance of 20 μrad. An optical mode tilt on the order of a tenth of a milliradian will produce an optical beam with approximately one MW of power and is considerably below the design tolerance of 0.1 μrad. This permits the FEL to be small enough to fit inside a ship, achieve at least a MW of power, and minimize the potential for resonator mirror damage.

Simulations predict the optimal design of a recirculating electron beam FEL with 100 MeV of energy has an undulator with approximately fifteen undulator periods, a Rayleigh length of a few cm, an outcoupling mirror which is roughly half transmissive. The optical and electron beams are both focused at the center of the undulator and the electron radius at the focus is only a fraction of a millimeter. The electron bunch length is about a third of a millimeter, and the electron bunch charge is approximately one nanocoulomb. Simulations predict these parameters will produce a MW class laser beam with a one micron optical wavelength.

FELs are a promising technology that the Navy projects will be available within the next decade. If this timeline holds, the next aircraft carrier, CVN-21, or destroyer, DD(X) flight 2, may be the first ship class to employ a high energy laser as a defensive weapon. A weapon system that provides a faster and more accurate response will prove to be a valuable asset to the Navy by giving ships an advantage over their adversaries. That advantage justifies the continued research in this technology required to make this futuristic weapon a reality.

LIST OF REFERENCES

[1] Albertine, John R., *High Energy Laser Weapons - Introduction and Overview*, PPT presentation at the Naval Postgraduate School. Monterey, California. May 2003.

[2] Blau, Joseph and Colson, W. B., Naval Postgraduate School, *FEL Modeling and Simulation*, PPT presentation at 2003 DEPS symposium.

[3] Blau, J., Bouras, V., Kalfoutzos, A., Allgaier, G., Fontana, T., Crooker, P. P., Colson, W. B., *Simulations of High-Power Free Electron Lasers with Strongly Focused Electron and Optical Beams*. FEL 2002 Conference Paper, September 2002.

[4] Behre, C. P. Jr., *Optical Cavity Mirror Stabilization*, Bachelors Thesis. Old Dominion University. Norfolk, Virginia. April 2002.

[5] Campbell, Thomas, *Simulations Of A Short Rayleigh Length 100 kW FEL And Mirror Stability Analysis*. Master's Thesis. Naval Postgraduate School. Monterey, California. December 2002.

[6] Colson, W. B., Pellegrini, C., and Renieri, A., *Classical Free Electron Laser Theory*, Chapter 5 in *Free Electron Laser Handbook*, Elsevier Science Publishing Co. Inc, 1990.

[7] Crooker, P. P., Campbell, T., Ossenfort, W., Miller, S., Blau, J., Colson, W. B., *A Study of the Stability of a High-Power Free Electron Laser Utilizing a Short Rayleigh Length*, FEL 2002 Conference Paper, September 2002.

[8] *EW & Radar Handbook, Radar Horizon/Line of Sight*. https://ewhdbks.mugu.navy.mil/rdr-hori.htm (December, 2003).

[9] FAS, Federation of American Scientists, Military Analysis Network http://www.fas.org, (December, 2003).
   a. *CVN-68 Nimitz-class* (January, 2000).
   b. *Moskit SS-N-22 Sunburn* (August, 1999).
   c. *RIM-7 Sea Sparrow Missile* (November, 1999).
   d. *RQ-1 Predator MAE UAV* (November, 2002).

[10] Jackson, *Classical Electrodynamics*, 2nd Edition, (October 1975).

[11] McGinnis, Roger, *Free Electron Laser Development For Directed Energy*.Ph. D Dissertation. Naval Postgraduate School. Monterey, California. December 2000.

[12] Ossenfort, William, *MegaWatt Class Free Electron Lasers for Naval Application—Short Rayleigh Length And Stability Analysis*. Master's Thesis. Naval Postgraduate School. Monterey, California. December 2002.

[13] Todd, Alan, Advanced Energy Systems, *Prior Workshop Report & Progress in System Concepts*, PPT presentation the Naval Postgraduate School. Monterey, California. April 18, 2003.

[14] Truver, Scott C., Naval warfare at the speed of light, Jane's Navy International, July 01, 2003.

[15] Wolfowitz, Paul. Commencement Address at the Naval War College, Remarks as Prepared for Delivery, Newport, Rhode Island, Friday, June 20, 2003. http://www.nwc.navy.mil/pao/Wolfowitz%20Commencement%20Address%20at%20the%20Naval%20War%20College%20June%2003.htm (December, 2003).

INITIAL DISTRIBUTION LIST

1. Defense Technical Information Center
   Ft. Belvoir, Virginia

2. Dudley Knox Library
   Naval Postgraduate School
   Monterey, California

3. Dr. Fred Dylla
   TJNAF
   Newport News, Virginia

4. CAPT Roger McGinnis, USN
   Naval Sea Systems Command
   CODE SEA 53R
   Washington Navy Yard, DC

5. Dr. George Neil
   TJNAF
   Newport News, VA

6. Dr. Alan Todd
   Advanced Energy Systems, Inc.
   Princeton, New Jersey

7. Dr. Gil Graff
   Office of Naval Research, Code 351
   Arlington, Virginia

8. Michael B. Deitchman
   Office of Naval Research, Code 531
   Arlington, Virginia

9. Professor William B. Colson
   Naval Postgraduate School
   Monterey, California

10. Professor Robert L. Armstead
    Naval Postgraduate School
    Monterey, California

11. Professor Joseph A. Blau
Naval Postgraduate School
Monterey, California

12. Professor Peter P. Crooker
Naval Postgraduate School
Monterey, California

13. Chairman, Physics Department
Naval Postgraduate School
Monterey, California

14. LT Gregory G. Allgaier, USN
Surface Warfare Officer Schools Command
Newport, Rhode Island